

POLISH
ACADEMY
OF SCIENCES

COMMITTEE
OF MACHINE
ENGINEERING

**SCIENTIFIC PROBLEMS
OF MACHINES OPERATION
AND MAINTENANCE**

ZAGADNIENIA EKSPLOATACJI MASZYN

TRIBOLOGY • RELIABILITY • TEROTECHNOLOGY
DIAGNOSTICS • SAFETY • ECO-ENGINEERING

TRIBOLOGIA • NIEZAWODNOŚĆ • EKSPLOATYKA
DIAGNOSTYKA • BEZPIECZEŃSTWO • EKONŻYNIERIA

2 (162)
Vol. 45
2010

Institute for Sustainable Technologies – National Research Institute, Radom

EDITORIAL BOARD:

Editor in Chief	Stanisław Pytko
Deputy Editor in Chief	Marian Szczerek
Editor of Tribology	Marian Szczerek
Editor of Reliability	Janusz Szpytko
Editor of Terotechnology	Tomasz Nowakowski
Editor of Diagnostics	Wojciech Moczulski
Editor of Safety	Kazimierz Kosmowski
Editor of Eco-Engineering	Zbigniew Kłos
Scientific Secretary	Jan Szybka
Secretary	Ewa Szczepanik

EDITORIAL ADVISORY BOARD

Bolesław Wojciechowicz (Chairman)

Alfred Brandowski, Tadeusz Burakowski, Czesław Cempel, Wojciech Cholewa, Zbigniew Dąbrowski, Jerzy Jaźwiński, Jan Kiciński, Ryszard Marczak, Adam Mazurkiewicz, Leszek Powierża, Tadeusz Szopa, Wiesław Zwierzycki, Bogdan Żółtowski

and

Michael J. Furey (USA), Anatolij Ryzhkin (Russia), Zhu Sheng (China), Gwidon Stachowiak (Australia), Vladas Vekteris (Lithuania).

Mailing address: Scientific Problems of Machines Operation and Maintenance
Institute for Sustainable Technologies – National Research Institute
ul. Pułaskiego 6/10, 26-600 Radom, Poland
Phone (48-48) 364 47 90
E-mail: ewa.szczepanik@itee.radom.pl

The figures have been directly reproduced from the originals submitted by the Authors.



CONTENTS

M. Trzos, D. Maldonado Cortés: The effect of the test condition on the scatter of the friction coefficient measurements	7
G. Szala: The modification of the generalised two-parametric fatigue characteristics based on Haigh diagram conception	19
M. Pająk: The space of a feature of a complex technical system	31
A. Katunin: Identification of multiple cracks in composite beams using discrete wavelet transform.....	41
L. Knopik: Mixture of distributions as a lifetime distribution of a technical object	53
M. Wrona: The application of the computer image analysis in wear particle research	61
H. Tomaszek, S. Stępień, M. Ważny: Aircraft flight safety with the risk of failure during performance of an aviation task	75
H. Tomaszek, J. Żurek, M. Ważny: Method of describing a catastrophic failure of an element of an aircraft	87

SPIS TREŚCI

M. Trzos, D. Maldonado Cortés: Wpływ parametrów procesu na rozrzut pomiarów współczynnika tarcia	7
G. Szala: Modyfikacja uogólnionej dwuparametrycznej charakterystyki zmęczeniowej opartej na koncepcji wykresu zmęczeniowego Haigha	19
M. Pająk: Przestrzeń cech złożonego systemu technicznego	31
A. Katunin: Identyfikacja wielopółeniowych pęknięć w belkach kompozytowych z zastosowaniem dyskretnej transformacji falkowej	41
L. Knopik: Mieszanina rozkładów jako rozkład czasów zużycia obiektu technicznego	53
M. Wrona: Zastosowanie komputerowej analizy obrazu w badaniach cząstek zużycia	61
H. Tomaszek, S. Stępień, M. Ważny: Bezpieczeństwo lotów statków powietrznych z ryzykiem awarii w czasie wykonywania zadania lotniczego	75
H. Tomaszek, J. Żurek, M. Ważny: Metoda opisu uszkodzenia katastroficznego elementu konstrukcji statku powietrznego	87

MAGDALENA TRZOS*, DEMÓFILO MALDONADO CORTÉS**

The effect of the test condition on the scatter of the friction coefficient measurements

Key words

Friction testing methods, unlubricated friction, friction coefficient, measurement reproducibility.

Słowa kluczowe

Metody badań tarcia, tarcie bezsmarowe, współczynnik tarcia, powtarzalność pomiaru.

Summary

The test results of friction coefficient measurement scatter are presented and evaluated. The friction coefficients of three different materials of friction couples under dry conditions were investigated. Ball-on-ring tests with both a vertical and a horizontal position of the sample axis and ball-on-disk tests for each friction couple were carried out in order to compare the tribotester influence on the scatter of results. The tribological experiment encompassed trials of different values of the friction process parameters: humidity, load, and velocity. The influences of process parameters on the scatter of results were analysed to assess the scatter level as a dependence on both tribotester and friction process parameters. Based on test results, the dependence between friction coefficient measurement scatter and load was revealed. The ratio of scatter to the measured friction coefficient was investigated. This error is dependent on scatter and also on the value of the friction coefficient; therefore, its value can change if the friction coefficient changes, e.g. along with humidity changes that were experimentally illustrated. As a result of the research, the conditions of the friction process, both of the low and high levels of error ratio, were predicted. The prediction was verified in the additional experiments.

* Institute for Sustainable Technologies – National Research Institute, ul. Pułaskiego 6/10, 26-600 Radom, Poland (e-mail: magdate@poczta.fm), phone: (48)361-42-41.

** University of Monterrey (UDEM), Mechanical Engineering Faculty, San Pedro Garza Garcia, Mexico.

1. Introduction

The key influence of the friction processes on the efficiency, reliability, and durability of produced and maintained machines and devices, on the one hand, and the lack of an uniform theory that explains the phenomenon in friction contacts on the other hand, make the experimental results the main source of information on the tribological properties of the object. Because of the multitude of theories relating to particular tribological problems, an array of experimental methods in tribology is observed. As the consequences of diverse research methods, the increasing number of tribotesters assigned to cause the specific tribological situation is developed. The analysis of friction and wear research results show the great differences of achieved results that characterise the same properties of investigated tribological objects and also the significant differences of result scatter are observed. The problem can be illustrated by the data presented in Santner's publication [1] who has collected friction coefficient values of steel – TiN couple that were achieved as the research results in a few dozen significant tribological centres in many parts of the world.

Since the analysis revealed the poor reproducibility of tribological experimental results, some of the international initiatives that aim to address the problem have been taken into consideration. The *Versailles Program on Advanced Materials and Standards VAMAS* was of great importance among them. However, the situation still remains unsatisfactory, mainly because tribological properties are not a feature of an individual material but of the friction couple materials and significantly dependent on friction contact configuration and friction process parameters.

Analysis in the scope of the VAMAS project [1, 2] have showed that reproducibility of ball-on-disk tests that depend on tribo-couple materials was quite good for pairs steel/steel and steel/coated disc but are really poor for coated ball/coated disk. Specific tribological behaviour may be different for different material pairs, and different for the material pair with or without electrical current [3]. The sample preparation is also of great importance and can influence friction data [4]. Wear particles and their exact behaviours in the contact area can affect friction in a stochastic and hence unpredictable way. The research on the influence of asperities on the instabilities of the sliding friction coefficient indicated that the extent of turbulent fluctuation of the friction coefficient could be reduced through increasing the nominal area [5]. Tribological research by Suzuki [6] indicated that the friction coefficient values depend on friction contact configuration; ball-on-disk tests gave a much higher coefficient of friction than roll/slide test. The results of the effects of load on the reproducibility of ball-on-disc test in the investigation of tin hard-coating indicated that friction behaviour characteristics of TiN sliding against aluminium surfaces is reproducible at different loads as long as the wear is confined within the TiN coating [7]. Investigation of tribological properties of

boron carbide coating against steel [8] revealed that a deviation less than 15% of the mean value was observed for the friction coefficient in a steady state that was obtained under medium and high humidity; whereas, the friction coefficient at low humidity was unstable.

The scatter of test results of the lubricated friction process can be caused by chemical effects. The chemistry of lubricant base stocks and additives do affect the fatigue life level and the scatter of fatigue life data. Furthermore, lubricant chemistry effects can vary with stress and slip (conditions controlled in the gear roller tests), and tests for lubricant chemistry effects should be conducted in conditions of importance to the application [9].

The fatigue durability scatter for different materials of friction contact and different lubricants was analysed in the research of friction contact fatigue durability predictions [10].

The objective of study, presented in this article, was to estimate the influence of the several factors, primarily, the type of tribotesters, humidity, load, and velocity influence on the scatter of friction coefficient values. The Taguchi method, which enables the reduction of the number of experiments, was applied to determine the suitable testing parameters in order to obtain a minimum of result scatter of the determined friction coefficient.

The Taguchi method, which combine the experiment design theory and the quality loss function concept have been widely utilised in engineering analysis. The Taguchi method [11] uses specially designed orthogonal arrays to study the entire parameter space with a finite number of experiments, saving experimental time, reducing cost, and enabling the identification of significant factors quickly. This method, among other things, succeeded to optimise the multiple tribological performance characteristics of Electroless Ni–P coatings [12] and was applied [13] to explore how the different parameters, such as drill shape and friction angle, friction contact area ratio, feed rate, and drilling speed would affect the response parameter.

2. Experiment description

The friction coefficient tests were conducted in the Institute for Sustainable Technologies – National Research Institute with the use of professional tribotester T-10 of ball-on-ring and T-11 of ball-on-disk friction couple [14]. Dry friction processes were carried out. The tribotesters, T-10 and T-11, were designed for the investigation of the basic tribological properties of materials. They both enable the measurement of the couple friction coefficient and the investigation of surface wear intensity during a friction process. They enable result registration every second. Specifically, the T-10 tribotester is designed for the estimation of tribological properties of materials for machine elements working in a sliding condition, especially in the case of thin coatings. With the use of the T-10 tribotester, the resistance to wear and the friction coefficient of

any materials working in slip friction contact can be precisely investigated in relation to their dependence on slip velocity, surface stress, and other factors. This tribotester is of two types: the vertical – T-10V with vertical friction contact and load configuration, and the horizontal – T10H with horizontal friction contact and load configuration (Fig. 1).



Fig. 1. Position of friction contact in T10 and T11 tribotesters
Rys. 1. Ustawienie węzła tarcia w testerach T10 i T11

Similarly, the T-11 tribotester is designed for the estimation of the tribological properties especially for the machine element materials used in sliding conditions. With the use of this tribotester, the friction coefficient and wear resistance of any friction couple materials working in sliding motion and their dependence on sliding velocity, surface stress, the type of gas in the testing chamber and others factors can be estimated. The T-11 tribotester is mounted with a vertical position of the friction couple and load. It was marked in this study by T-11V.

In the scope of the investigations presented in this article, the comparison of the friction coefficient measurements with the use of different but professional tribotesters is presented.

Three different friction contact materials were investigated in experiments of different process parameters, namely: load, velocity, and humidity. The scatter of the friction coefficient was studied, and the degree of the influence of couple materials and process parameters on scatter were analysed. The friction coefficient μ and friction coefficient scatter act as dependent variables.

The research encompassed combinations of factors, each of three levels, as shown in Tab. 1.

Tab. 1. Process parameters and theirs levels
Tab. 1. Parametry procesu oraz ich wartości

Levels	Process parameters			
	Couple's materials (M)	Humidity (H) [%]	Load (P) [N]	Speed (v) [m/s]
1	steel* disc –steel* ball (S/S)	35	5	0.1
2	steel* disc –ceramic** ball (S/C)	50	10	0.2
3	coated*** disc –ceramic** ball (P/C)	80	15	0.3

*AISI 52100, ** Al2O3, ***CrN

The same friction processes with the same combinations of factor values were repeated on different tribotesters: (T-10H, T-10V, and T11-V), and the friction distance for one process was constant and equalled 1000 m. The friction force was registered every one second during the process.

Taking under consideration the above assumptions, the large numbers of experimental investigations have to be carried out, namely, 243 experiments that need a lot of time and at significant costs. To solve this problem, the settings of friction process parameters were determined by using the Taguchi experiment design method.

In accordance with the Taguchi optimisation method, nine friction experiments were designed and, an L9, an orthogonal array was constructed, which had nine rows corresponding to the number of tests, as shown in Table 2. Each trial (process) presented in Tab. 2 recurred five-times for each of the three tribotesters.

The average scatter of measurements in experimental results is also included in Tab. 2.

Tab. 2. Values of process parameters and scatter of test results for individual tribotesters
Tab. 2. Wartości parametrów procesu oraz rozrzutu wyników badań dla poszczególnych tribotesterów

Trial no.	Process parameters				Measurements' average scatter for tribotester		
	M	H [%]	P[N]	v[m/s]	T10H	T10V	T11V
1	S/S	35	5	0.1	0.069	0.133	0.126
2	S/S	50	10	0.2	0.170	0.029	0.052
3	S/S	80	15	0.3	0.084	0.018	0.133
4	S/C	35	10	0.3	0.092	0.04	0.099
5	S/C	50	15	0.1	0.102	0.035	0.031
6	S/C	80	5	0.2	0.155	0.079	0.082
7	P/C	35	15	0.2	0.038	0.121	0.111
8	P/C	50	5	0.3	0.142	0.085	0.195
9	P/C	80	10	0.1	0.115	0.032	0.163

Average scatter and average friction coefficients based on five measurements were calculated. The scatter was calculated as the average value of the differences between each of five measurements.

The samples were properly prepared with the use of an ultra vibration-cleaning machine for cleaning with a benzene solvent.

3. Results and discussion

The results of the analysis of the tribological experiments indicate certain differences among the values of the measured friction coefficients as recorded

on different tribological test devices, even though the same condition of friction processes were present. However, the achieved results proved that the differences were small with the exception of Trial No. 8, using the T-11 tribotester. Analysis of the process and experimental results (Fig. 2) indicate that the differences in measurements on different tribotesters did not depend on the materials of friction contact and process parameters. One of the smallest differences was observed for Trial Number 3 (contact material – steel – steel). The largest difference was observed in Trial Number 8, if the friction coefficient value measured on the T-11V tribotester is compared with the results achieved on the T-10V and on T-10H tribotesters. In that case, the differences of average value were above 0.25, while in the other cases, were less than 0.1.

The next analysis concerned the estimation of the influence of individual variables, namely: friction couple materials and process parameters on the scatter of the friction coefficient. The average values of scatter were calculated independently for each variable for individual tribotesters.

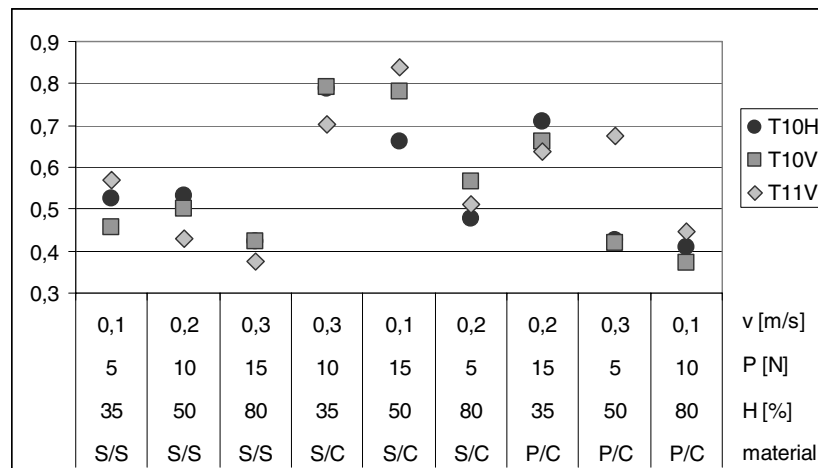


Fig. 2. Average values of the friction coefficient as the result of measurements on different tribological devices and different process parameters

Rys. 2. Wartości średnie współczynników tarcia zmierzonych z użyciem poszczególnych tribotesterów przy różnych wartościach parametrów procesu

The conducted research confirmed the influence of tribotester on the scatter of friction coefficients (Fig. 3). Actually, the smallest scatter was observed in the ball-on-ring investigation on the T-10V tribotester with the vertical position of the sample's axis of rotation. That scatter was even above threefold smaller in comparison with others. According to the research results (Fig. 3), the materials of the friction couple have an influence on the results scatter achieved on different tribological devices. The similar scatter on different tribotesters was observed for the friction coefficient of steel-ceramic couple and the differences were below 0.07, while for other materials, they were about twofold higher.

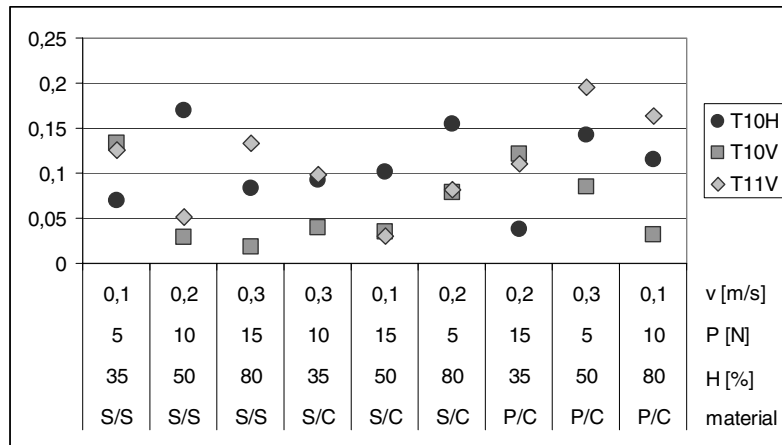


Fig. 3. Average scatters of friction coefficients on different devices and process parameters

Rys. 3. Wartości średnie rozrzutów współczynników tarcia wyznaczonych z użyciem poszczególnych tribotesterów przy różnych wartościach parametrów procesu

However, it should be pointed that, beside the absolute value of scatter in the reproducibility analysis, the scatter should be linked to the value of the friction coefficient. Therefore, additional analysis of this type was carried out to estimate the scatter influence on the error of friction coefficient measurements. To measure that influence, the coefficient b_{μ} was established as the ratio of average values of scatter to the average values of the friction coefficient:

$$b_{\mu} = r/\mu$$

Where, r is the average value of scatter (calculated as the average value of differences between each of five measurements), μ - average value of friction coefficient.

The analysis of error share, caused by scatter, in the calculated average value of friction coefficients revealed the influence of both the test devices and process parameters. As with the absolute value of scatter, the smallest b_{μ} coefficient was observed on the T-10V tribotester. The average value of b_{μ} for that tester was 12%, while for each of the other two, it was above 20%.

In order to estimate the influence of the considered, in the scope of research, parameters on share of scatter in the calculated average value of friction coefficients, the calculations were done for the b_{μ} average value for individual variables: speed, humidity, load, and the friction couple materials. The calculation results are presented in Figs. 4, 5, and 6.

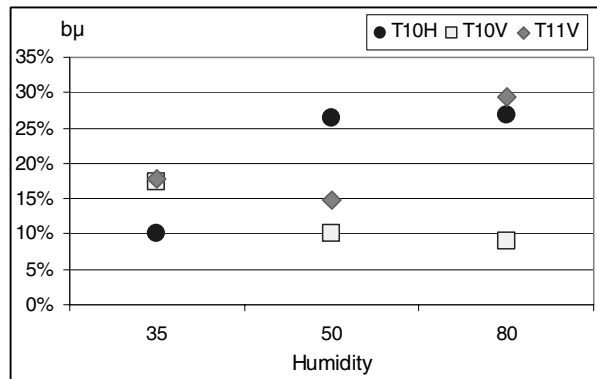


Fig. 4. Values of b_μ coefficient for different humidities [%] and different tribotesters
 Rys. 4. Wartości współczynnika b_μ przy różnych wartościach wilgotności dla poszczególnych tribotesterów

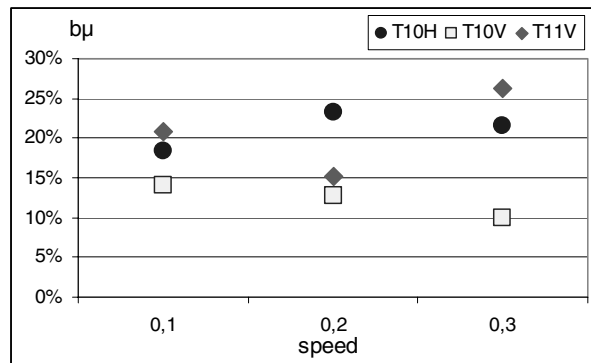


Fig. 5. Values of b_μ coefficient for different speeds [m/s] and different tribotesters
 Rys. 5. Wartości współczynnika b_μ przy różnych wartościach prędkości dla poszczególnych tribotesterów

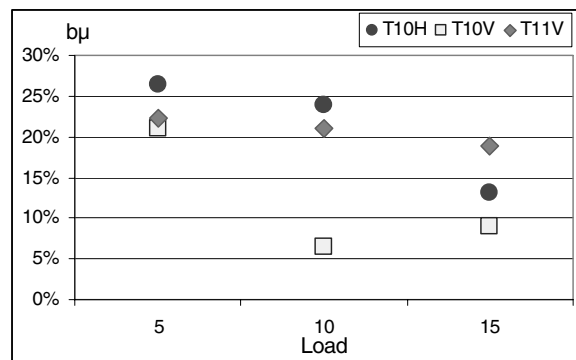


Fig. 6. Values of b_μ coefficient for different loads [N] and different tribotesters
 Rys. 6. Wartości współczynnika b_μ przy różnych wartościach obciążenia dla poszczególnych tribotesterów

The similarities of load influence on the b_{μ} coefficient were noticed for all tribological devices, namely, the decrease of the coefficient while the load increases. That tendency is particularly well illustrated in Fig. 7, where load dependence on result scatter for individual friction couple materials is presented.

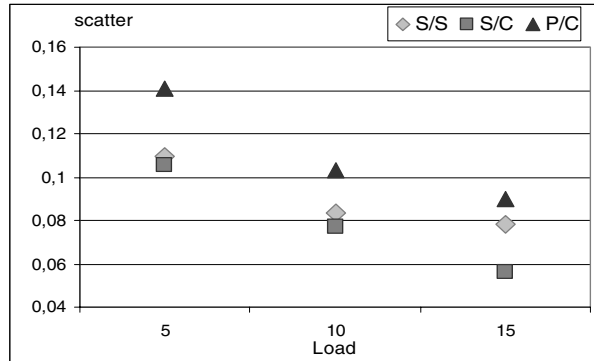


Fig. 7. Friction coefficient scatters for the different materials of friction couple and different loads [N]

Rys. 7. Rozrzut pomiarów współczynnika tarcia dla różnych materiałów pary tarcia i różnych obciążeń

As can be seen (Fig. 5), velocity has a low influence on result scatter. In case of T-10V tribotester, for which the smallest scatter is observed, along with an increase in humidity, is a decrease in the test result scatter. However, the increase of the ratio scatter to friction coefficient in case of the T-10H and T-11V tribotesters (Fig. 4), while the 50% and 80% values of humidity are considered, resulted from the change in the friction character and the decrease of friction coefficient values. This is well illustrated in Fig. 8 and 9 by the examples of changes of the friction coefficient and result scatter on T-11V and T-10H in the dependence of humidity.

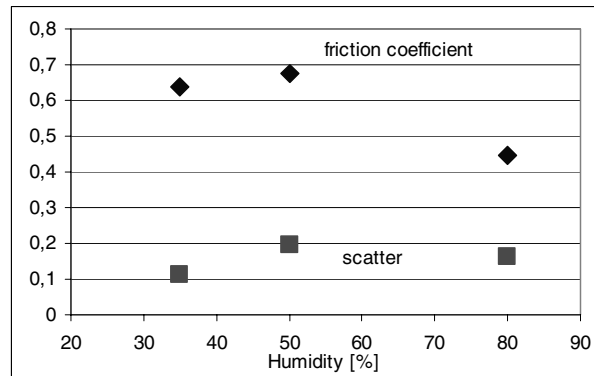


Fig. 8. The average values and average scatter of the friction coefficient of P/C materials measured on T-11V

Rys. 8. Średnia wartość i średni rozrzut współczynnika tarcia skojarzenia materiałowego P/C zmierzonego na tribotesterze T-11V

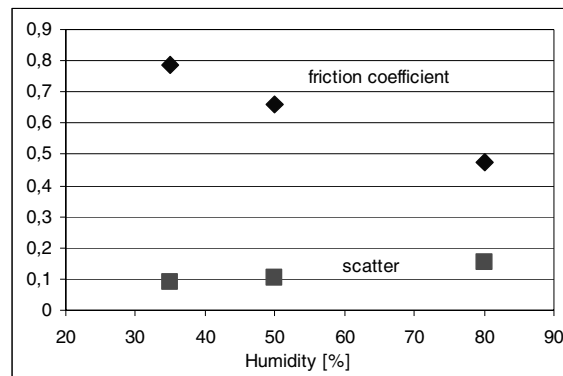


Fig. 9. The average values and average scatter of friction coefficient of S/C materials measured on T-10 H

Rys. 9. Średnia wartość i średni rozrzut współczynnika tarcia skojarzenia materiałowego S/C zmierzonego na tribotesterze T-10 H

In all analysed cases, we did not notice a scatter dependence on humidity; however, humidity influences the friction coefficient value and consequently the b_{μ} coefficient.

The particular analysis of experimental results revealed that measurement scatter of the friction coefficients of investigated materials, with the use of three tribotesters, does not depend on humidity and velocity but on load.

In order to verify the observed, on the basis of experimental results, influence of the noticed parameters on the scatter of friction coefficient, two additional experiments were conducted: one with a low predicted level of scatter and another with a high predicted level of scatter. The values of parameters for each of the verification processes are presented in Tab. 3. The b_{μ} values achieved as the result of verification are also presented.

Tab. 3. Friction process parameters and b_{μ} values achieved as the result of verification
Tab. 3. Wartości parametrów procesu tarcia i b_{μ} uzyskane w rezultacie badań weryfikacyjnych

Predicted scatter level	Process parameters					scatter share in measured friction coefficient b_{μ} [%]
	Tribotester	Couple's materials	Humidity [%]	Load [N]	Speed [m/s]	
low	T10V	steel–ceramic (S/C)	50	10	0.1	7
high	T11V	coated steel –ceramic (P/C)	50	5	0.3	31

Each of the verification processes was repeated three times, and the average values of the friction coefficient and scatter were calculated. The verification results proved both high (0.16) and low (0.07) friction coefficient scatter predicted based on previous analysis. Therefore, the possibility of scatter level

prediction and, as consequence of prediction, the planning research with low scatter, for example, increasing the number of experiment repetitions while predicted scatter level is high was indicated.

4. Conclusions

On the basis of friction coefficient measurements conducted on different testers for different materials and friction process parameters, the main conclusion are summarised as follows:

- (1) The differences in result reproducibility on different tribotesters were revealed. A ball-on-ring tester with a vertical position of rotation axis (T-10V) had the smallest value of scatter and scatter share in the friction coefficient value compared with other investigated testers.
- (2) Despite the differences of the reproducibility of results, the average values of friction coefficient measured with the use of different testers were comparable, while the materials of couple and friction parameters were the same.
- (3) The friction coefficient scatter decreases with increasing load. That regularity was proved for all analysed tribotesters in the scope of friction parameters and friction couple materials investigated.
- (4) From the test results, the humidity influence on scatter was not noticed. However, the change of the friction coefficient with the change of humidity may cause a change of scatter share in the friction coefficient measured value.
- (5) The test results analysis did not prove scatter dependence on velocity.
- (6) The identified relation of result scatter and factors that were analysed enabled the estimation of friction coefficient scatter level depending on friction process parameters. This information can support the research planning in a way that enables a possible small share of scatter in the measured values of the friction coefficient.

Acknowledgements: This research was sponsored by Polish Ministry of Science and Higher Education, under grant Number 2865/B/T02/2009/37.

References

- [1] E. Santner, Comparison of wear and friction measurements of TiN coatings, *Tribologia* 1/95 (1995) 7–29.
- [2] H. Czichos, S. Becker, J. Lexow, International multilaboratory sliding wear tests with ceramics and steel, *Wear* 135 (1989) 171–191.
- [3] H. Zhao, G.C. Barber, J. Liu, Friction and wear in high speed sliding with and without electrical current, *Wear* 249 (2001) 409–414.
- [4] K.C. Ludema, *Friction, wear, and lubrication – a textbook in tribology*, Boca Raton (Florida), CRC Press (1996).

- [5] H. Zhai, Z. Huang, Instabilities of sliding friction governed by asperity interference mechanisms, *Wear* 257 (2004) 414–422.
- [6] M. Suzuki, Comparison of tribological characteristics of sputtered MoS₂ films coated with different apparatus, *Wear* 218 (1998) 110–118.
- [7] M.Z. Huq, J. P. Celis, Reproducibility of friction and wear results in ball-on-disc unidirectional sliding tests of TiN-alumina pairings, *Wear* 212 (1997) 151–159.
- [8] P.D. Cuong, H.-S. Ahn, E.S. Yoon, K.H. Shin, Effects of relative humidity on tribological properties of boron carbide coating against steel, *Surface & Coatings Technology* 201 (2006) 4230–4235.
- [9] W. Castro, D.E. Weller, K. Cheenkachorn, J.M. Perez, The effect of chemical structure of base fluids on antiwear effectiveness of additives, *Tribology International* 38, (2005) 321–326.
- [10] M. Trzos, W. Piekoszewski, R. Ruta, The number of research courses influence on the estimation of friction contact fatigue durability scatter of lubricated rolling contacts. *Tribologia* 230, (2010) 163–175.
- [11] W.H. Yang, Y.S. Tarn, Design optimization of cutting parameters for turning operations based on the Taguchi method, *J Mater Process Technol* 84, (1998) 122–129.
- [12] P. Sahoo, S.K. Pal, Tribological Performance Optimization of Electroless Ni–P Coatings Using the Taguchi Method and Grey Relational Analysis, *Tribol Lett* 28, (2007) 191–201.
- [13] H.M. Chow, S.M. Lee, L.D. Yang, Machining characteristic of friction drilling on AISI 304 stainless steel, *Journal of materials processing technology* 207, (2008) 180–186.
- [14] D. Maldonado, Influence of test parameters on the coefficient of friction, *Tribologia* 222, (2008) 83–92.

Manuscript received by Editorial Board, January 15th 2010

Wpływ parametrów procesu na rozrzut pomiarów współczynnika tarcia

Streszczenie

Zaprezentowano rezultaty badań rozrzutów współczynnika tarcia. Badania przeprowadzono dla trzech różnych skojarzeń materiałowych w warunkach tarcia suchego. Przeprowadzono testy z użyciem tribotestera z węzłem kula–pierścień zarówno z poziomą, jak i pionową pozycją osi węzła oraz tribotestera z pionową pozycją ustawienia osi węzła kula–tarcza w celu porównania wpływu urządzenia badawczego na rozrzut wyników badań. Eksperyment tribologiczny obejmował różne wartości parametrów procesów tarcia: wilgotności, obciążenia oraz prędkości. Przeanalizowano wpływ parametrów procesu na rozrzut wyników badań, aby ocenić poziom rozrzutu w zależności zarówno od urządzenia, jak i parametrów procesu. Na bazie uzyskanych rezultatów wykazano zależność rozrzutu wyników pomiaru współczynnika tarcia od obciążenia. Analizie poddano również współczynnik szacujący błąd wynikający z udziału rozrzutu w wyznaczonej wartości współczynnika tarcia. Udział tego błędu zależy zarówno od rozrzutu wyników, jak również od wartości samego współczynnika tarcia, dlatego też jego wartość może się zmieniać wraz ze zmianą wartości współczynnika tarcia, np. na skutek zmiany wilgotności, co zostało eksperymentalnie wykazane i zilustrowane. W wyniku przeprowadzonych badań i analizy wyników wyznaczono warunki pomiarów współczynnika tarcia zarówno o niskim, jak i wysokim poziomie rozrzutu wyników pomiaru. Przeprowadzone eksperymenty weryfikacyjne potwierdziły prognozowane poziomy rozrzutów.

GRZEGORZ SZALA*

The modification of the generalised two-parametric fatigue characteristic based on haigh diagram conception**Key words**

Fatigue life, two-parametric characteristics, S355J0 steel.

Słowa kluczowe

Trwałość zmęczeniowa, dwuparametryczne charakterystyki zmęczeniowe, stal S355J0.

Summary

The experimental verification of the generalised two-parametric fatigue characteristics has shown good compatibility between the calculation and the fatigue life examination results with use of constant amplitude load and variable asymmetry coefficients, according to the model based on the Haigh diagram conception. The level of compatibility depended on the durability range, and it decreased considerably for the low durability values (high-tension values).

The analysis of the experimental verification results indicated that the significant factor having an influence on the level of compatibility between the calculation and examination results is the material stress sensitivity coefficient that is present in the mathematical model. In this work, the modification of the generalised two-parametric fatigue characteristics based on the Haigh diagram conception, based on example of steel S355J0 examination, is presented.

* University of Technology and Life Sciences in Bydgoszcz Prof. Kaliskiego Street 7, 85-789 Bydgoszcz, Poland, tel.: +48 52 340 82 95, fax: +48 52 340 82 71; e-mail: gszala@utp.edu.pl

Nomenclature:

A	–	elongation in %,
C	–	constant in formula describing the S-N curve for the fluctuating stress ($R = 0$),
C_0	–	constant in formula describing the S-N curve for the alternating stress ($R = -1$),
N	–	the number of cycles general designation (fatigue life),
N_0	–	the number of cycles of the fatigue life corresponding to fatigue limit,
$R = S_{\min} / S_{\max}$	–	the stress ratio,
R_e	–	material plasticity limit in MPa,
R_f	–	general fatigue limit designation in MPa,
R_m	–	tensile strength in MPa,
R_0	–	fatigue limit for fluctuating stress ($R = 0$) for the number of cycle N_0 in MPa,
R_0^N	–	fatigue limit for the sinusoidal fluctuating stress ($R = 0$) for the number of cycles N in MPa,
R_{-1}	–	fatigue limit for the alternating stress ($R = -1$) for the number of cycles N_0 in MPa,
R_{-1}^N	–	fatigue limit for the sinusoidal alternating stress ($R = -1$) for the number of cycles N in MPa,
S	–	general stress designation in the specimen in MPa,
$S_a = 0,5(S_{\max} - S_{\min})$	–	stress amplitude in the sinusoidal cycle in MPa,
$S_m = 0,5(S_{\max} + S_{\min})$	–	the mean stress in the sinusoidal cycle in MPa,
$S_{\max} = S_m + S_a$	–	the maximum stress in the sinusoidal cycle in MPa,
$S_{\min} = S_m - S_a$	–	the minimum stress in the sinusoidal cycle in MPa,
Z	–	contraction in %,
m	–	exponent in the formula describing the S-N curve for the fluctuating stress ($R = 0$),
m_0	–	exponent in the formula describing the S-N curve for the alternating stress ($R = -1$),
Ψ	–	material stress sensitivity coefficient for $N = N_0$,
Ψ_N	–	material stress sensitivity coefficient for $N \neq N_0$.

1. Introduction

In work [1] the need to determinate the two-parametric fatigue characteristic in the calculations of fatigue life of the structural components, which, in the operation, conditions, have been subjected to random loads of a wide spectrum has been widely substantiated. Additionally, experimental verification has been made of the Heywood characteristics [2] and five models.

The models are marked with Roman numerals: I, II, III, IV, and V. From the experimental verification carried out on the specimens made of S355JO steel, it turned out that Model I has a lot of merits and that the compatibility between the calculation results of fatigue life according to this model and the examination results, apart from the low durability range ($N = 10^2 - 10^4$), is satisfactory, which corresponded to the high levels of the variable stresses.

The similar conclusions can be formed regarding examinations described the work [3] on the specimens made of D16CzATW aluminium air alloy. From the analysis of the verification results, it appeared that the material stress sensitivity coefficient ψ_N is the factor that has the significant impact on the compatibility between the calculation results and the examination results.

The aim of this work is to modify the generalised two-parametric fatigue characteristic based on the Haigh diagram conception, which means assuming a suitable relation between the value of the material stress sensitivity coefficient ψ_N and its fatigue life. The modified characteristics have been experimentally verified on the specimens made of S355JO steel.

2. Formulation of the problem

In work [1], the description of two-parametric fatigue characteristic $N(S_a, S_m)$ is given – Model I in the following form:

$$N = \frac{N_0 R_{-1}^{m_0}}{(S_a + \psi_N S_m)^{m_0}} \quad -\infty < R \leq 0 \quad (1)$$

and

$$N = N_0 \left[\frac{R_{-1}(R_m + S_a - S_m)}{S_a R_m (1 + \psi_N)} \right]^{m_0} \quad 0 < R \leq 1.0 \quad (2)$$

or, in the form which is more convenient to draw a contour line diagram (the contour line corresponds with the condition of the constant durability N for variables S_a and S_m):

$$\frac{S_a}{R_m} = -\psi_N \frac{S_m}{R_m} + \frac{R_{-1}}{R_m} \left(\frac{N_0}{N} \right)^{\frac{1}{m_0}} \quad -\infty < R \leq 0 \quad (3)$$

and

$$\frac{S_a}{R_m} = \frac{R_{-1}}{R_m \left(\frac{N}{N_0} \right)^{\frac{1}{m_0}} (1 + \psi_N) - R_{-1}} \left(1 - \frac{S_m}{R_m} \right) \quad 0 < R \leq 1.0 \quad (4)$$

In this article, the impact of the ψ_N coefficient on the fatigue calculations according to the formulas given above are the subject of the analysis.

The $\psi_N = \psi$ coefficient in various publications, e.g. [4], and it is dependent on the material and on the type of variable load. For example, for bending in extreme cases: $\psi = 0.07 - 0.23$, for axial load: $\psi = 0.05 - 0.19$, and for torsion: $\psi = 0 - 0.14$. The values in the low range apply to low-strength steel (e.g. steel 10), whereas the values in the high range apply to high-strength steel (e.g. thermally improved steel 36HNM).

For the high cycle fatigue (HCF), Formula [5] enables one to calculate the sensitivity coefficient of a material for $N \neq N_0$ ($\psi_N \neq \psi$), and the following form has been derived:

$$\psi_N = 2C_0^{\frac{1}{m_0}} C^{-\frac{1}{m}} N^{\left(\frac{1}{m} - \frac{1}{m_0}\right)} - 1 \quad (5)$$

The application of the given relation to Formulas (1) to (4) causes the difference in the fatigue calculation results and the examination results, especially for the number of cycles N in the range $10^2 - 10^4$, which has been pointed out in work [6]. Therefore, a more beneficial solution is the application of the experimental relation described by the following Formula in work [5], which has already been mentioned:

$$\psi_N = N^k \quad (6)$$

where k is the index exponent dependent on the material and variable load type.

The modification of Model I of the two-parametric fatigue characteristic means replacing the analytic solution to the stress sensitivity coefficient of a material ψ_N according to Formula (5) with the experimental relation Formula (6)

3. The experimental verification of modified Model I of the two-parametric fatigue characteristic $N(S_a, S_m)$

The modified two-parametric fatigue characteristic are marked in the following text as an IM model.

3.1. The calculation and examination results for steel S355JO

The static properties of steel S355JO are in Table 1, and the cyclic properties are in Table 2.

Table 1. The static strength properties of steel S355JO
Tabela 1. Statyczne własności wytrzymałościowe stali S355JO

	The static properties of steel S355JO				
	R_e	R_m	E	A_5	Z
	MPa	MPa	MPa	%	%
Average value	499.9	678.0	208159	17.2	59.8
Standard deviation	8.4	7.1	1306	0.99	0.9

Table 2. The cyclic mechanical properties of steel S355J0
Tabela 2. Cykliczne własności mechaniczne stali S355J0

Load type	equation form	Exponent	Absolute term	Fatigue limit	
				R _f	N ₀
Alternating (R=-1)	$S_a^{m_0} \cdot N = C_0$	m ₀ = 12.33	C ₀ = 1.156·10 ³⁶	R ₋₁ = 274	10 ⁶
Fluctuating (R=0)	$S_{max}^{m_0} \cdot N = C$	m = 15.92	C = 6.163·10 ⁴⁸	R ₀ = 480	10 ⁶

From the data contained in work [5], the index exponent k in the Formula (6) is equal 0.1586.

The static and cyclic properties given above and the value of the index exponent k enables one to make fatigue calculations of the two-parametric fatigue characteristic according to Formulas 3, 4 and 6. These formulas for the analysed steel and data contained in Tables 1 and 2, after necessary transformation, assume the following form:

– Formula 1:

$$N = 10^{36} \frac{1,14147}{\left[S_a \left(1 - \psi_N \frac{R+1}{R-1} \right) \right]^{12,33}} \quad (1a)$$

– Formula 2:

$$N = 1,14147 \cdot 10^{36} \left[\frac{678 + S_a \frac{2R}{1-R}}{678 S_a (1 + \psi_N)} \right]^{12,33} \quad (2a)$$

– Formula 3:

$$S_a = \frac{840}{N^{0,081} \left(1 + \psi_N \frac{R+1}{R-1} \right)} \quad (3a)$$

– Formula 4:

$$S_a = \frac{185772}{221,14(1 + \psi_N) + 274 \frac{2R}{1-R}} \quad (4a)$$

The results of the fatigue calculations, according to formulas given above for various stress values are depicted in the Table 3.

Column 2 depicts the values of the stress ratio coefficient, column 3 – N durability in cycles, for which the amplitude value S_a corresponding to fatigue strength of the specimen R_{-1}^N has been calculated. Column 4 shows the values of the material stress sensitivity coefficient calculated with use of Formula (6). Data from columns 2 through 4 provide the fatigue calculation for Model I (column 5) and for the model after the modification IM (column 6) possible. In order to compare the calculated values S_{ac} with the experimental data S_{aex} , the data from the examination derived from work [6] have been presented in column 7 of Table 3.

4. Analysis of the results of calculations and their experimental verification

The data contained in Table 3 can provide a graph of the two-parametric fatigue characteristics in the form of the contour line diagram. In Fig. 1, the following diagrams are depicted:

- a – characteristics diagram according to Model I (column 5, Table 3),
- b – characteristics diagram according to the modified IM model (column 6, Table 3),
- c – diagram according to the experimental data (column 7, Table 3).

From the comparison of the diagrams, it turns out that the calculations, both for Model I and the modified IM model, result in higher values than the experimental ones. The only exceptions are the data for the stress sensitivity coefficient $R = -1.0$, for which the compatibility is total, which results from the assumptions accepted by the model design.

Table 3. The results of the fatigue calculations according to Model I and IM as well as experimental data for S355JO steel

Tabela 3. Wyniki obliczeń zmęczeniowych według modelu I i IM oraz dane doświadczalne dla stali S355JO

Lp.	R	N	Ψ_N	Calculations S_a acc. to model		Experimental data S_{aex}
				I	IM	
1	2	3	4	5	6	7
1	-3.0	10^4	0.23	448.4	449.0	350.0
2		10^5	0.162	361.8	359.4	300.0
3		10^6	0.115	292.4	290.7	265.0
4		10^7	0.08	236.7	236.5	250.0
5	-2.0	10^2	0.465	-----	-----	-----
6		10^3	0.35	-----	-----	-----
7		10^4	0.23	430.3	431.3	385.9
8		10^5	0.162	350.6	349.1	336.7
9		10^6	0.115	285.9	285.1	293.8

Lp.	R	N	Ψ_N	Calculations S_a acc. to model		Experimental data S_{aex}
				I	IM	
10		10^7	0.08	233.5	233.3	256.4
11	-1.25	10^2	0.465	600.4	609.8	559.2
12		10^3	0.35	495.0	449.2	475.0
13		10^4	0.23	408.3	399.1	403.5
14		10^5	0.162	336.8	336.4	343.1
15		10^6	0.115	277.9	277.5	291.1
16		10^7	0.08	229.3	229.0	247.6
17	-1.0	10^2	0.465	578.3	578.3	578.7
18		10^3	0.35	479.8	480.3	480.2
19		10^4	0.23	398.1	398.5	398.4
20		10^5	0.162	330.3	330.6	330.5
21		10^6	0.115	274.0	274.3	274.2
22		10^7	0.08	227.3	227.6	227.5
23	-0.5	10^2	0.465	500.7	500.8	473.6
24		10^3	0.35	439.2	429.7	419.4
25		10^4	0.23	370.3	369.8	371.4
26		10^5	0.162	312.1	313.4	328.9
27		10^6	0.115	263.0	264.0	291.2
28		10^7	0.08	221.5	221.1	257.9
29	0.0	10^2	0.465	434.1	394.7	433.5
30		10^3	0.35	375.6	355.4	375.5
31		10^4	0.23	325.1	323.6	324.9
32		10^5	0.162	281.3	284.2	281.2
33		10^6	0.115	243.4	245.7	243.3
34		10^7	0.08	210.6	210.5	210.6
35	0.5	10^2	0.465	289.6	182.4	175.0
36		10^3	0.35	261.9	173.5	165.0
37		10^4	0.23	237.8	165.1	151.0
38		10^5	0.162	216.9	154.6	149.0
39		10^6	0.115	199.0	142.5	136.0
40		10^7	0.08	183.6	130.0	125.0

Designation: R – the stress ratio $R = S_{min}/S_{max} = (S_m - S_a)/(S_m + S_a)$
 Ψ_N – material stress sensitivity coefficient

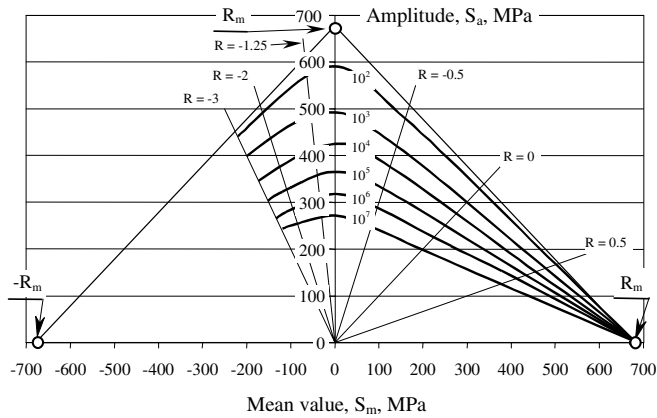
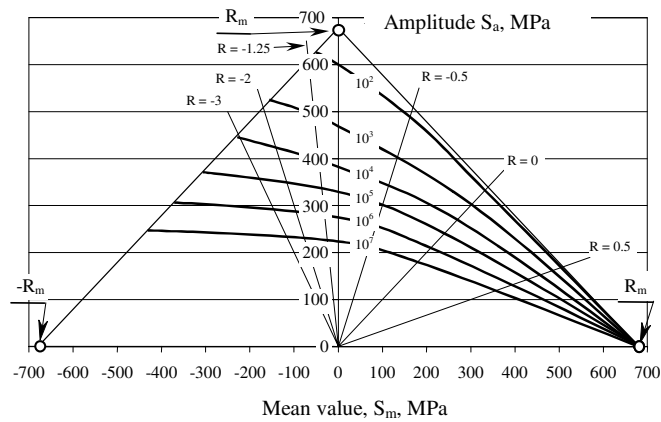
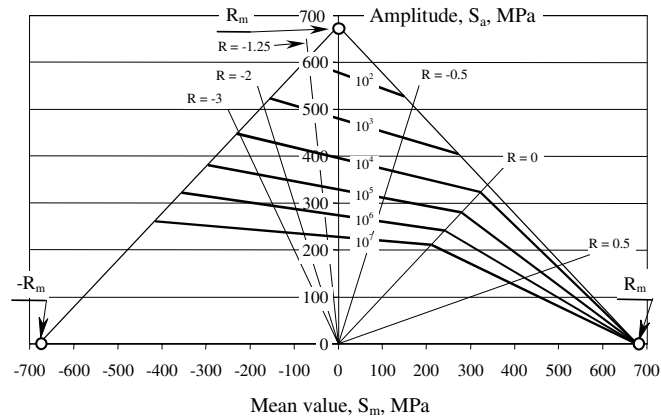


Fig. 1. Contour line diagrams of the two-parametric fatigue characteristics for the steel S355JO: a – according to Model I, b – according to the modified IM model, c – diagram determined on the base of experimental data

Rys. 1. Wykresy warstwiczne dwuparametrycznych charakterystyk zmężeń dla stali S355JO: a – według modelu I, b – według zmodyfikowanego modelu IM, c – wykres wyznaczony na podstawie danych doświadczalnych

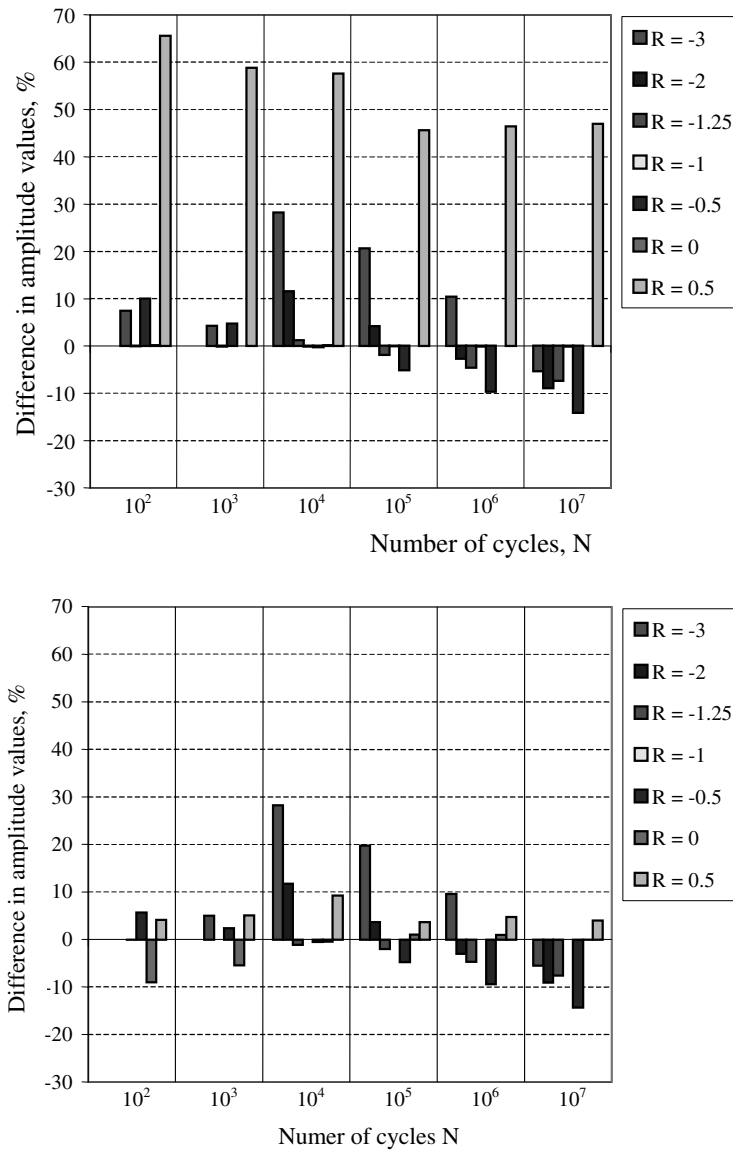


Fig. 2. Relative difference of the fatigue strength calculated and determined experimentally:
a – for Model I, b – for IM model

Rys. 2. Względna różnica wytrzymałości zmęczeniowej obliczonej i wyznaczonej doświadczalnie:
a – dla modelu I, b – dla modelu IM

Please notice that the shape of the diagram is determined using the experimental examination for the cycles with a negative average value (on the side of compressive stress). It is generally assumed that the negative values of the average stress S_m , increase the S_a amplitude values.

The methods to increase the fatigue durability of structural components with preload and technological treatment, introducing compressive stress in the cracking area are based on this assumption. The discussed observation requires further research supplemented with metallographic examination.

When the results of the calculations from Model I and the modified IM model are compared, their high compatibility in the range of the variability of the coefficient R from (-0.5) to (-3.0), and significant differences in the range of variability of the coefficient R from 0 to 1.0 are observed. The results of the calculations from the modified IM model are closer to the experimental data in this range.

The quantitative evaluation of the differences between the calculation and experimental examinations results has been carried out by introducing a relative difference measure calculated according to the following formula:

$$\delta = \frac{S_{ac} - S_{aex}}{S_{aex}} \cdot 100\% \quad (7)$$

The illustration of relative differences calculated according to Formula (7) is depicted in the Fig. 2. From the diagram (Fig. 2), it turns out that the maximal relative difference values δ are 65 % and apply to R= 0.5 and strength range N from 10^2 to 10^3 apply to Model I (Fig. 2a) and for 28 % R= -3 from...and N 10^4 – model IM (Fig. 2b).

From the data it turns out that especially in the range of the coefficient R variability from 0 to 1,0, as it was given above, the compatibility of the model IM calculation results with the experimental data is higher than in the Model I.

5. Conclusions

- The quantitative relative differences between the calculation and experimental examination results for different values of the material stress sensitivity coefficient R (-3; -2; -1.25; -1; -0.5; 0; 0.5) and different strength values N (10^2 , 10^3 , 10^4 , 10^5 , 10^6 , 10^7) show that the results closer to experimental ones are received in calculations with use of the IM (modified) model. The significant improvement of the compatibility between the calculation and experimental examination results is observed for the values of R in the range 0 through 1.0. In the remaining ranges, the relative differences in the stress calculated according to comparable models are small.
- The application of the IM model in the fatigue calculation is more significantly beneficial, because the material stress coefficient value is calculated from empirical Formula (7). Therefore, it is not necessary to know

the parameters of the S-N curve for the cycle asymmetry coefficient $R = 0$ (fluctuating stress), which is necessary in the basic Model I, because the value of the material stress sensitivity coefficient is being calculated from Formula (5). Data about the S-N curve for various materials and for coefficient $R = -1$ (alternating stress) are widely available in publications, but data for the S-N curve for coefficient $R = 0$, are rare.

- The two-parametric fatigue characteristics have significant merits in the calculation of the service fatigue life in cases of broadband random service stress. Using these conditions, developed stress spectra are characterised by considerable dispersion of amplitude S_{ai} and average S_{mi} values of the sinusoidal cycles. In this situation, it is significant to evaluate the impact of the analysed differences between the models of the two-parametric fatigue characteristics on the calculated fatigue life. There are some cases in which small differences in the fatigue diagrams caused considerable differences in calculated fatigue life. The analysis of this problem is a subject for further research and calculations, which will be presented in the next publications.

References

- [1] Ligaj B., Szala G.: Experimental verification of two-parametric models of fatigue characteristics by using the tests of S355J0 steel as an example, Polish Maritime Research, 1, 10, 2010.
- [2] Heywood R. B.: Designing Against Fatigue, Chapman Hall, London 1962,
- [3] Szala J., Lipski A.: A conception of descriptions of fatigue material properties in fatigue life calculations of structural elements, Zagadnienia Eksploatacji Maszyn, 22, 2005.
- [4] Kocańda S., Szala J.: Fundamentals of fatigue calculations (in Polish), PWN, Warszawa 1997.
- [5] Szala G.: Material sensitivity coefficient on stress cycles asymmetry in high cycles fatigue (HCF), Problemy eksploatacji, Radom 2010.
- [6] Szala G., Ligaj B.: Research of cycle asymmetry ratio influence on steel S355J0 fatigue life, Proceedings of XXIII Symposium on Fatigue and Fracture Mechanics, Bydgoszcz 2010.

Manuscript received by Editorial Board, June 30th 2010

Note: This work has been elaborated in the frame of the project No. 0715/B/T02/2008/35 financed by Polish Ministry of Sciences and Higher Education.

Modyfikacja uogólnionej dwuparametrycznej charakterystyki zmęczeniowej opartej na koncepcji wykresu zmęczeniowego Haigha

Streszczenie

Weryfikacja doświadczalna uogólnionych dwuparametrycznych charakterystyk zmęczeniowych wykazała dobrą zgodność wyników obliczeń z wynikami badań trwałości zmęczeniowej w warunkach obciążenia stałoamplitudowego i zmiennych współczynników asymetrii według modelu opartego na koncepcji wykresu zmęczeniowego Haigha. Poziom zgodności zależny był od zakresu trwałości i istotnie obniżał się dla niskich trwałości (wysokich wartości naprężeń).

Analiza wyników weryfikacji doświadczalnej wskazywała na to, że istotnym czynnikiem wpływającym na poziom zgodności wyników obliczeń i badań ma występujący w modelu matematycznym współczynnik wrażliwości materiału na asymetrię cyklu. W tej pracy przedstawiona zostanie modyfikacja uogólnionej dwuparametrycznej charakterystyki zmęczeniowej opartej na koncepcji wykresu zmęczeniowego Haigha na przykładzie badań stali S355JO.

MICHAŁ PAJAŁ*

The space of a feature of a complex technical system

Key words

Exploitation, maintenance management, complex technical systems, state of a system.

Słowa kluczowe

Sterowanie eksploatacją, złożone systemy techniczne, stan systemu.

Summary

During the exploitation phase, the operating and service processes take place on one technical object. They can be performed at the same time or in sequence. Therefore, in an exploitation system, there is an exploitation conflict. The main reason for this is a dependence of operating and service activities and the limitation of access to the technical object. To solve the described problem, the operating and service processes have to be managed together. It means that exploitation processes should be executed according to a maintenance strategy, which defines a moment in time when operation processes should be finished and the object should be intended for service. This moment depends on the system state. Simultaneously, the system state is one of the main factors, which determinates a method of operation and service processes. Therefore, the system state is the most important variable in a process of maintenance control. It should be noticed that the system state is determined by values of the system cardinal features. In this paper, a feature's space of a complex exploitation system is defined. Additionally, different types of a feature's space are described. Next, the state of the system is formulated as a point of the defined space. Proposed interpretation is a base for a projection of the system state changes taking place during different exploitation process execution in the space of one common feature. Thanks to this, the implementation of a coherent mathematical method of the maintenance control process description will be possible.

* Radom University of Technology, Faculty of Mechanical Engineering, Department of Thermal Technology 26-600 Radom, ul. Krasickiego 54, Poland; phone: (48) 48 361 71 49, e-mail: m.pajak@pr.radom.pl

1. Introduction

System concept is one of the most basic and general concepts used in different domains of science. There are many definitions of this concept, which can be found in different publications, for example, in [1–6]. The most suitable definition for the purpose of these studies is one that describes the system as an ordered triple $\langle E, R, \emptyset \rangle$ which consists of a set of E elements, R sequence (a relation on elements from E set), and a set of \emptyset objectives realised by the system. E is called the set of elements, R – it is a structure, and \emptyset is the objective function. Despite the differences between the definitions, each of them uses the set of system elements and the relation between them.

The object of presented studies is a complex, hierarchical exploitation system with technical objects as its elements. Technical objects are identified by their features: qualities and properties. The quality of the object is the feature that is specified only based on knowledge of the object. The loss of object qualities means that object is no longer the same but becomes another one [7]. A property of technical object is a relative feature. It is defined based on its relation to the objects of the environment. Due to property, it is possible to distinguish some objects from the others without that property [8]. Based on object features, we can treat it as a part of set of system elements. Technical object features can be divided into two groups: additive and constitutive. Additive features are independent from relations inside the system, but constitutive ones depend on it [9]. System features resulted from additive features of its elements can be defined as a sum of features of particular system elements. Unfortunately, in case of constitutive features of the system, this way of defining is not proper. Therefore, to identify the system itself, it is necessary to determine the unique set of the system features.

2. The state of features and subspace system states

It is possible to distinguish two types of system features -- measurable and non-measurable ones [10]. As far as non-measurable features are concerned, it is not possible to measure their values because of technical difficulties or because of a lack of researcher knowledge [11]. In order to determine the approximate value of non-measurable features, a range of variability can be assigned. The range of variability is divided homogeneously into m parts described by m values. These values correspond to the intensity of the appearance of an approximated feature. Due to the range of variability implementation, it is possible to express the intensity of the feature between 0 and m values.

Independently from a type of a system's feature x_i , the range of its variability X_{iZM} can be defined as a set of values that the feature can have. The range of variability is limited by its minimum value x_{imin} and its maximum value

x_{imax} . Inside the range of feature variability, depending on chosen criteria, we can distinguish boundary minimum and maximum values (x_{igrmin} and x_{igrmax}) which describe the range of acceptable values.

The subset of the acceptable values that is limited by the suboptimal minimum value x_{isomin} and suboptimal maximum value x_{isomax} is called the suboptimal values range. Among the suboptimal values, it is possible to distinguish the optimal value x_{io} . In defining presented values, the following ranges are formulated (1-4) (Fig. 1).

$$X_{iZM} = \langle x_{imin}, x_{imax} \rangle \quad (1)$$

$$X_{iND} = \langle x_{imin}, x_{igrmin} \rangle \cup \langle x_{igrmax}, x_{imax} \rangle \quad (2)$$

$$X_{iD} = \langle x_{igrmin}, x_{igrmax} \rangle \quad (3)$$

$$X_{iSO} = \langle x_{isomin}, x_{isomax} \rangle \quad (4)$$

- Where: X_{iZM} – variability range of a system's feature i,
 x_{imin}, x_{imax} – minimum and maximum value of a system's feature i,
 X_{iND} – range of unacceptable values of a system's feature i,
 x_{igrmin}, x_{igrmax} – boundary minimum and boundary maximum value of a system's feature i,
 X_{iD} – range of acceptable values of a system's feature i,
 x_{isomin}, x_{isomax} – suboptimal minimum and suboptimal maximum value of a system's feature i,
 X_{iSO} – range of suboptimal values of a system's feature i.

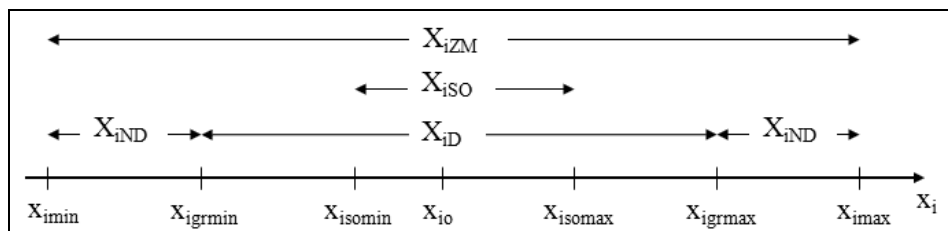


Fig. 1. Variability range of a system's feature
 Rys. 1. Przedział zmienności cechy opisującej system

It was stated that the characteristic values of a feature are the values that determine the variability range of the feature and its subsets of unacceptable,

acceptable, and suboptimal values as well as characteristic ranges of the feature, which are the range of variability and unacceptable, acceptable and suboptimal values range of the feature.

If the following set of variables

$$X = \{x_i, i = 1, \dots, n\} \quad (5)$$

is enough for identifying the system, then the system state is a set of temporary values of X variables [12]. The elements of this set are called state variables and their values for a specified moment are called state coordinates [13]. The state variables identify the system, so they are equal to the subset of system features. This subset is defined as a set of cardinal features. Based on the definitions of a state [14], [15], it was defined that a set of cardinal features is the smallest set of the system features which are important for the considered issue. The temporary values of the cardinal features uniquely identify the system state.

The system state, described by vector of cardinal features (state vector)

$$X = [x_1, x_2, \dots, x_n]^T \quad (6)$$

can be interpreted as a point in an n -dimensional space, where n is the cardinality of the set of cardinal features. N -dimensional space is called the space of features of the system. In Fig. 2, the space of features of a system and a system state point for $n = 2$ is presented.

If we interpret points of the feature's space of the system as the system states, then characteristic ranges of the system features (1 - 4) determine n -dimensional subspaces of the system states in a feature's space. The ranges of unacceptable values of the system features determine the subspace of unacceptable system states S_{ND} . The ranges of acceptable values of the system features determine the subspace of acceptable system states S_D ; whereas, the ranges of suboptimal values determine the subspace of suboptimal system states S_{SO} . The subspaces of the system states in a feature's space are constructed as the Cartesian product [16], which is an intersection of cylindrical extensions of enumerated ranges of the system features (7, 8).

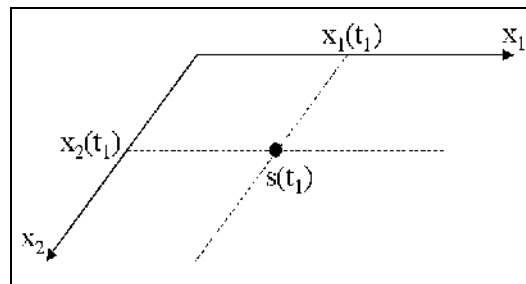


Fig. 2. State of the system in t_1 moment in a space of features $[x_1, x_2]$
Rys. 2. Stan systemu s dla chwili t_1 w przestrzeni cech systemu $[x_1, x_2]$

$$\rho(\pi_{x_1}(R)) = \{(x_1, x_2) \in X_1 \times X_2 : x_1 \in \pi_{x_1}(R)\} \quad (7)$$

$$\rho(\pi_{x_2}(R)) = \{(x_1, x_2) \in X_1 \times X_2 : x_2 \in \pi_{x_2}(R)\} \quad (8)$$

Where: R – relation at $X_1 \times X_2$,
 $\pi_{x_n}(R)$ – projection of the relation R on set X_n ,
 $\rho(\pi_{x_n}(R))$ – cylindrical extension of X_n set.

3. Types of spaces of features of a system

Characteristic values of the system feature i can be dependent or independent from the values of others features of the system. Independent system features are the features that have independent characteristic values; consequently, dependent system features have dependent characteristic values.

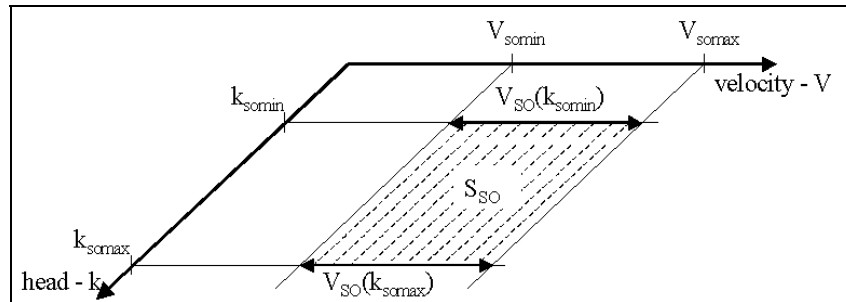


Fig. 3. Subspace of suboptimal system states in a space of two independent features
 Rys. 3. Obszar stanów suboptymalnych systemu w przestrzeni dwóch cech niezależnych

As an example of independent features, we can consider velocity and head of a motor-driven vessel. These two features describe the state of an exploitation system of the vessel. Zero and the maximum value of vessel speed limit the range of variability of the „velocity” feature. Inside the range of variability, the minimum boundary value can be distinguished which is equal to its manoeuvring speed, and the maximum boundary speed can be defined. This is a highest speed of the vessel allowed by legal regulations [17]. This is also possible to indicate the maximum and minimum suboptimal values, which are equivalent to the minimum and maximum value of the highest engine efficiency. Omitting waves, sea currents, and wind force influence, the characteristic values of „velocity” feature are independent from the vessel head. For this example, subspace of suboptimal system states is a rectangle in a two-dimensional feature’s space (Fig. 3).

The example of dependent features is temperature and the absolute humidity of air, which define a state of a working medium of a ventilation system in a building [18]. The range of variability for the temperature is limited by the minimum value and maximum value decreased by 5°C [19] defined for external air for a specific climatic zone [20]. Inside the variability range the minimum boundary value is equal to temperature of the anti-freezing program of heating installation and it is equal to 6°C [21]. The maximum boundary value is equal to the maximum value of variability range. The purpose of ventilation in a room is keeping the heat comfort conditions, which are described by temperature and air absolute humidity [22]. Consequently, the minimum and maximum suboptimal values of feature „temperature” in the presented example are equal to boundary values in the range of the heat comfort area. According to standards [23], these values depend on an absolute humidity of air.

It means that, depending on the value of the „absolute humidity” feature, the boundaries of suboptimal values of the „temperature” feature change [24]. For this example, the subspace of suboptimal states of the system in the two-dimensional space of a feature is presented below (Fig. 4).

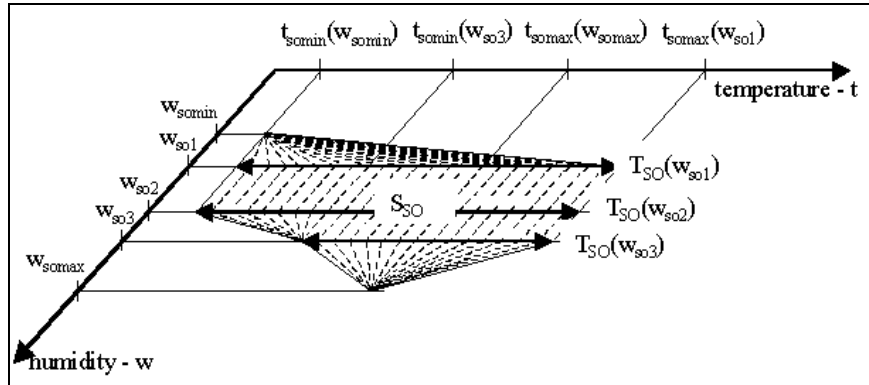


Fig. 4. Subspace of suboptimal system states in a space of two dependent features
Rys. 4. Obszar stanów suboptymalnych systemu w przestrzeni dwóch cech zależnych

Subspaces of a system states defined above in two-dimensional space of features, in case of n-dimensional space are expressed as hyperspaces R^n (9)

$$H(R^n) = \{(x_1, x_2, \dots, x_n) \in R^n : a_1 \leq x_1 \leq b_1 \wedge a_2 \leq x_2 \leq b_2 \wedge \dots \wedge a_n \leq x_n \leq b_n\} \quad (9)$$

where: $H(R^n)$ – hyperspace R^n ,
 a_n, b_n – boundary values in dimension no. n,
 x_1, x_2, \dots, x_n – coordinates of points in R^n space.

If boundary values of hyperspaces in particular dimensions fulfil the conditions (10, 11), then the features of the system are independent ones and hyperspaces R^n become to be hypercubes R^n [25].

$$\begin{bmatrix} \frac{\partial a_1}{\partial x_1} & \frac{\partial a_1}{\partial x_2} & \dots & \frac{\partial a_1}{\partial x_n} \\ \frac{\partial a_2}{\partial x_1} & \frac{\partial a_2}{\partial x_2} & \dots & \frac{\partial a_2}{\partial x_n} \\ \vdots & \vdots & \ddots & \vdots \\ \frac{\partial a_n}{\partial x_1} & \frac{\partial a_n}{\partial x_2} & \dots & \frac{\partial a_n}{\partial x_n} \end{bmatrix} = 0 \quad (10)$$

$$\begin{bmatrix} \frac{\partial b_1}{\partial x_1} & \frac{\partial b_1}{\partial x_2} & \dots & \frac{\partial b_1}{\partial x_n} \\ \frac{\partial b_2}{\partial x_1} & \frac{\partial b_2}{\partial x_2} & \dots & \frac{\partial b_2}{\partial x_n} \\ \vdots & \vdots & \ddots & \vdots \\ \frac{\partial b_n}{\partial x_1} & \frac{\partial b_n}{\partial x_2} & \dots & \frac{\partial b_n}{\partial x_n} \end{bmatrix} = 0 \quad (11)$$

If conditions (10, 11) are not fulfilled, then features creating the space of features R^n of the system are dependent ones. Their characteristic values are changing concurrently with the values of correlated features. It implies the creation the hyperspaces of the system states in R^n space, which are more complicated in shape than hypercubes R^n .

The hypercubes R^2 for two independent features are presented in Figure (Fig. 5). The optimal state of the system s_O and real state of the system s_R are also presented.

Based on the definition of cardinal set of features, we can state that it consists of different elements depending on the analysed problem. A different set of cardinal features implies a different space of system features. Consequently, the system state treated as a point in a space of features can belong to different subspaces of system states depending on the space of features in which the state is described.

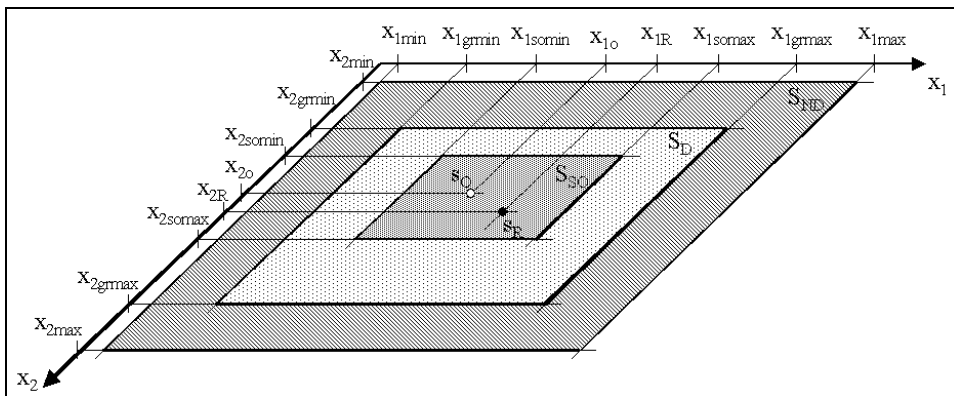


Fig. 5. Subspaces of system states presented in the independent space of features R^2
 Rys. 5. Obszary stanów systemu przedstawione w przestrzeni R^2 cech niezależnych

Due to the system state interpretation as a point in a space of features, it is possible to express the changes of system state during the exploitation phase as a trajectory of a system state point in its space of features. Additionally, defining subspaces of ability states, inability states, and limited ability states of the system, it is possible to estimate a risk of inability state appearance by analysis of the distance between points in n -dimensional space. It can be the basis of the mathematical methods implementation in the area of the management of maintenance processes in complex technical systems.

5. Conclusions

Based on the considerations presented in the paper, the following conclusions were formulated:

- Characteristic values of feature are defined as values that determine the feature variability range and subsets of its unacceptable, acceptable, and suboptimal values.
- Characteristic ranges of the feature are the following: variability range, unacceptable value range, acceptable value range, and suboptimal value range.
- The set of cardinal features is the smallest set of the system's features, which are important for the considered issue, and its temporary values uniquely identify the system state.
- System state described by a vector of cardinal features can be interpreted as a point in an n -dimensional space, where n is the cardinality of the set of the cardinal features. N -dimensional space is called the space of features of the system.

- Subspaces of system states in a space of a feature are constructed as Cartesian products, which are the intersections of cylindrical extensions of the ranges of the system's features.
- Independent features of a system are the features that have independent characteristic values; consequently, dependent features of a system have dependent characteristic values.
- The system state treated as a point in a space of features can belong to different subspaces of system states, depending on the space of features in which the state is described.
- The system state interpretation as a point in a space of features can be the basis of the implementation of mathematical methods in the area of the management of maintenance processes in complex technical systems.

References

- [1] Bojarski W.W., Podstawy analizy i inżynierii systemów, Warsaw, WNT, 1984.
- [2] Klir J., Vallach M., Cybernetic Modeling, New York 1967.
- [3] Ursul A., Priroda informacji, Moscow 1968.
- [4] Lesiński S., Jakość i niezawodność, Wydawnictwo ATR w Bydgoszczy, Bydgoszcz 1996.
- [5] Żółtowski B., Ćwik Z., Leksykon diagnostyki technicznej, Wydawnictwo ATR w Bydgoszczy, Bydgoszcz 1996.
- [6] Oziemski S., Efektywność eksploatacji maszyn. Podstawy techniczno-ekonomiczne, ITeE, Radom 1999.
- [7] Dietrych J., System i konstrukcja, WNT, Warsaw 1985.
- [8] Smalko Z., Podstawy eksploatacji technicznej pojazdów, Oficyna Wydawnicza Politechniki Warszawskiej, Warsaw 1998.
- [9] Bertalanffy L., Ogólna teoria systemów, PWN, Warsaw 1984.
- [10] Woropay M., Istotność a ograniczenie rozmyte, „Postępy Cybernetyki”, Ossolineum, Zeszyt 3/1984.
- [11] Klawitera A., Nowak L., Odkrycie, abstrakcja, prawda, empiria, historia, idealizacja, PWN, Warsaw – Poznan 1979.
- [12] Powierża L., Zarys inżynierii systemów bioagrotechnicznych, ITeE, Radom – Płock 1997.
- [13] Sawik T., Analiza i synteza wielowymiarowych układów sterowania, Wydawnictwo AGH, Cracow 1984.
- [14] Woropay M., Podstawy racjonalnej eksploatacji maszyn, ITeE, Bydgoszcz – Radom 1996.
- [15] Woropay M., Muślewski Ł., Jakość w ujęciu systemowym, ITeE, Radom 2005.
- [16] Ehrenfeucht A., Stande O., Algebra, PWN, Warsaw 1984.
- [17] International Maritime Organization, „International Regulations for Avoiding Collisions at Sea”, 1972.
- [18] Recknagel H., Sprenger E., Honmann W., Schramek E., Poradnik – ogrzewanie, klimatyzacja, EWFE, Gdańsk 1994.
- [19] PN-76/B-03421. Parametry obliczeniowe powietrza wewnętrznego w pomieszczeniach przeznaczonych do stałego przebywania ludzi. Wentylacja i klimatyzacja.
- [20] PN-76/B-03420. Parametry obliczeniowe powietrza zewnętrznego. Wentylacja i klimatyzacja.

- [21] Krygiel K., Klinke T., Sewerynik J., Ogrzewnictwo, wentylacja, klimatyzacja, WSiP, Warsaw 2007.
- [22] Gaziński B., Technika klimatyzacyjna dla praktyków, Systherm, Poznań 2005.
- [23] Norma DIN1946 .
- [24] Stoecker I., Kretschmar H.J., Mollier H-S Diagram for Water and Steam, Springer, 2008.
- [25] Kaku M., Hiperprzestrzeń – wszechświaty równoległe, pętle czasowe i dziesiąty wymiar, Warsaw 1997.

Manuscript received by Editorial Board, August 11th 2010

Przestrzeń cech złożonego systemu technicznego

Streszczenie

W fazie eksploatacji system techniczny występuje zarówno w procesie użytkowania, jak i obsługi zachodzących równocześnie lub po sobie. Powstaje wówczas konflikt wobec zależności działań oraz ograniczoności dostępu do obiektu technicznego. W celu rozwiązania konfliktu eksploatacyjnego procesy użytkowe i procesy zapewnienia zdatności muszą być procesami łącznie organizowanymi. Oznacza to, że w celu prowadzenia eksploatacji obiektu technicznego w sposób racjonalny, koniecznym jest zastosowanie strategii eksploatacyjnej określającej chwilę zakończenia procesów użytkowania i przekazania systemu do obsługi. Chwila ta wyznaczana jest na podstawie stanu systemu. Jednocześnie stan systemu jest również jednym z podstawowych czynników wpływających na sposób przeprowadzania procesów użytkowania i obsługi. Stan systemu jest zatem podstawową zmienną w procesie sterowania eksploatacją. Stan systemu z kolei jest opisany wartościami cech kardynalnych systemu. W opracowaniu zdefiniowano pojęcie przestrzeni cech systemu oraz omówiono rodzaje takich przestrzeni. Następnie przedstawiono stan systemu jako punkt zdefiniowanej przestrzeni. Zaproponowana interpretacja stanu systemu stanowi podstawę do wyrażania zmian stanu systemu zachodzących w trakcie realizacji odmiennych procesów eksploatacyjnych w jednej wspólnej przestrzeni jego cech. Podejście takie umożliwia zastosowanie spójnego aparatu matematycznego do opisu procesu sterowania eksploatacją złożonych systemów technicznych.

ANDRZEJ KATUNIN*

Identification of multiple cracks in composite beams using discrete wavelet transform

Key words

Faults identification, polymeric laminates, discrete wavelet transform.

Słowa kluczowe

Identyfikacja uszkodzeń, laminaty polimerowe, dyskretna transformata falkowa.

Summary

A method for the identification of multiple cracks based on Discrete Wavelet Transform is presented. The analysis is provided on beams made of polymeric laminate. The estimation of the crack locations is based on the evaluation of natural modal shapes of pre-cracked beams. The modal shapes were estimated experimentally using laser Doppler vibrometry. The dynamic response of multi-cracked beams is processed using Discrete Wavelet Transform and detail coefficients are considered for the crack identification. Next, the methods of detail coefficients denoising are discussed. The principles of the selection of the appropriate wavelet are investigated. The proposed method indicates effectiveness in multiple crack identification and could be applied in industrial solutions of structural health monitoring as well.

1. Introduction

The development of the novel applications of polymeric composites determines the necessity of their diagnosing during exploitation. During

* Department of Fundamentals of Machinery Design, Faculty of Mechanical Engineering, Silesian University of Technology, Konarskiego 18A, 44-100 Gliwice, Poland, e-mail: andrzej.katunin@polsl.pl

workloads, such structures were subjected to several fault initiations. The most typical faults that occurred in composites are cracks. The cracks may occur in different conditions, such as intensive loading, impacts, mechanical and thermal fatigue, etc. Considering the importance of some applications of composite structures, e.g. aircraft elements, diagnosing must be effective, non-destructive, and possibly low-cost and simple. The timely detection and identification of cracks may prevent breakdowns and makes possible appropriate repairs. In practice, one can observe the simultaneous initiation of multiple cracks. When multiple cracks appear in the structure, their dynamic response becomes more complex, taking into consideration their positions. Considering structural properties and loading conditions, cracks may propagate in a different manner. Therefore, the identification method must allow for the identifying of all presented cracks.

One of the most widespread groups of non-destructive methods in technical diagnostics is based on the modal analysis of the structures and specific techniques of signal processing. In the diagnostics of the structural health, many techniques based on measured signal transforms could be used. Some publications [1, 2] on crack detection in composite beams were based on Fast Fourier Transform (FFT); however, such analysis allows only the detection of the crack. Other techniques, which were used for crack detection, contain Short-Time Fourier Transform, kurtosis analysis, cepstrum-based techniques, etc. In the case of an early phase of the damage, the analysis of natural frequencies or signal point features variability often is not effective, and it is impossible to localise the crack and to estimate its dimensions. In this case, the changes in natural frequencies and modes are not directly detectable and require specific processing.

To fulfil the above-mentioned criteria, it is advisable to use multi-resolution techniques, e.g. Wavelet Transform (WT). This technique has some advantages, like the possibility of the application of different wavelets and the simultaneous scaling and shifting of them for approximation purposes. Many researchers use WT for crack identification. The problem of faults detection and isolation in composite beams in the early damage phase using Continuous Wavelet Transform (CWT) was studied and discussed [3]. This problem was also investigated by Douka *et al.* for beams with single [4] and double [5] cracks. They used symlets in CWT for identifying crack locations and the estimation of their relative depth. Research on the damage detection was provided by the research group of Ostachowicz. The authors presented several approaches in damage identification. They used experimental measurements and finite element models for identify cracks based on the deflection profiles [6]. In [7], the Discrete Wavelet Transform (DWT) was used for the crack identification. The authors compared the effectiveness of the identification using different wavelets. DWT on modal shape data used for crack identification allows one to separate the signal into the approximation coefficients and details coefficient

parts. Then, the details coefficients part is analysed to identify the damage. This procedure is quite quick and simple, which is an unquestionable advantage of DWT. However, the usage of wavelets in DWT is limited to compactly-supported orthonormal wavelets. Some studies concentrated on theoretical modelling of cracked or multi-cracked beam-like structure response, mainly using Galerkin formulation. The analytical model for Timoshenko beams proposed in [8] allows crack detection and localisation. Another valuable work [9] presents the finite element formulation for multi-cracked shafts.

In solving the problem of damage detection and identification using WT, it is important to select the appropriate wavelet. In previous works [10, 11], the problem was studied and several wavelets were compared. It was noticed that B-spline wavelets applied for damage detection give the best results in comparison with other wavelets both using CWT and DWT. The present paper deals with the method of multiple crack detection and identification in polymeric layered composite beams. In Section 2, the algorithm of single-level DWT will be presented for decomposition and reconstruction operations. In the next section, the parameters of the experimental study and the measurement equipment will be shown. Obtained measurements will be analysed for crack detection and an estimation of their depth. The selection of the appropriate wavelet for the analysis and parameters for detail coefficients filtering will be discussed. The filtering threshold was determined in terms of measurement noise and disturbances that result from vanishing moments of the applied wavelet.

2. The algorithm of Discrete Wavelet Transform and its inversion

The effectiveness of DWT is due to the dyadic bases of scales and translation positions, which makes possible the multi-resolution analysis. The algorithm was proposed by Mallat in [12]. The process of DWT is based on the decomposition of the signal $f(x)$ into the summation of wavelet bases at different dyadic scales. The decomposition of the signal is the filtering operation with the use of two filters, where the first one is the wavelet scaling function $\varphi(x)$ (low-pass filter) and the second one is the wavelet function $\psi(x)$ (high-pass filter). The signal $f(x)$ can be presented as the following relation:

$$f(x) = \sum_{n=-\infty}^{n=\infty} f_n^0 \varphi(x-n) \quad (1)$$

The operation of the decomposition considering (1) and the orthogonality of φ can be presented as follows:

$$f_n^{(j)} = \sum_k h_{2n-k} f_k^{(j-1)}, \quad d_n^{(j)} = \sum_k g_{2n-k} f_k^{(j-1)} \quad (2)$$

where j is the level of the decomposition and h and g are related to the low-pass filter and high-pass filter, respectively. After this operation, one can obtain the approximation coefficients f and the detail coefficients d as a result of the high-pass and low-pass filtering, respectively. Note that, after this operation, the resolution of the filtered signal is reduced twice.

The operation of the discrete signal reconstruction is based on Inverse Discrete Wavelet Transform (IDWT). Here the high-pass filter is applied to approximation coefficients, and the low-pass filter is applied to the detail coefficients. Then the convolution operation is used for the filtered coefficients. For the n -th level of reconstruction IDWT can be presented as follows:

$$f_n^{(j-1)} = \sum_k h_{k-2n} a_k^{(j)} + \sum_k g_{k-2n} d_k^{(j)} \quad (3)$$

The effectiveness of above-presented algorithms is strongly dependent on the analysing wavelet, which will be investigated and discussed later.

3. Experimental setup and measurements

3.1. Specimens and measurement equipment

The specimens were manufactured from glass-fibre reinforced epoxy in the form of unidirectional preimpregnated fibres. The specimens were prepared to achieve transversal isotropic properties. Layers orientation and characteristic material properties of the laminate may be found in [13]. The dimensions of specimen are as follows: length $L = 0.25$ m, width $W = 0.025$ m, and thickness $H = 0.005$ m. In the experiment, four specimens were considered, where the first one was undamaged and others were artificially pre-cracked. The cracks were created at various distances and with various depths. The positions and depth dimensions of the cracks are presented in Fig. 1. Considering the clamp of the specimen and the excitation clamp on the other side of the specimen, an additional dimension was defined as the effective length $L_{\text{eff}} = 0.215$ m on which the measurements are provided.

We provide the measurements using scanning laser vibrometer Polytec PSV-400 and the second point laser vibrometer Polytec PDV-100 was used as a measurement reference. The specimens were excited by the electrodynamic modal shaker TIRA TV-51120 by the random noise signal, which was amplified by the power amplifier TIRA BAA 500. The experimental stand was illustrated in Fig. 2. On the measurement surface of the specimens, the reflecting tape was attached to provide the satisfactory focus and power of the laser beam. Then, using PSV software, we defined 39 measurement points on L_{eff} with the constant interval of ~ 0.0055 m between them. The frequency bandwidth was set in the range of 0 to 2 kHz with the resolution of 0.625 Hz and the sampling frequency

equals 5.12 kHz. During the measurements, the velocity of vibrations in each defined point was measured.

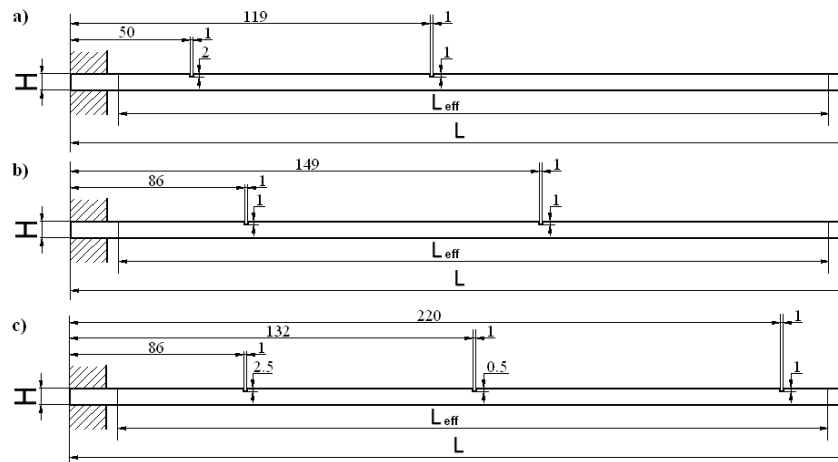


Fig. 1. Crack positions and depths in the investigated specimens
Rys. 1. Położenia i głębokości pęknięć w badanych próbkach

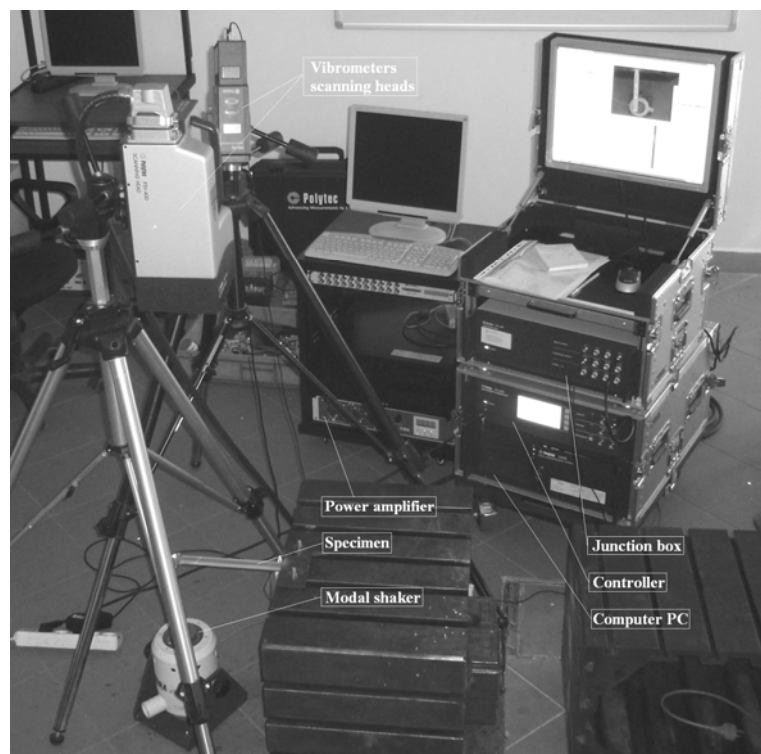


Fig. 2. Experimental setup
Rys. 2. Stanowisko eksperymentalne

3.2. Measurement data preprocessing

As a result of measurements, we obtain the Frequency Response Functions (FRF) for each specimen. Then, we select peaks on the FRF (see Fig. 3) for determining the natural frequencies and modal shapes of the investigated beams. It was necessary to separate only bending frequencies for further analysis. The first three bending, natural frequencies for all specimens are tabulated in Table 1.

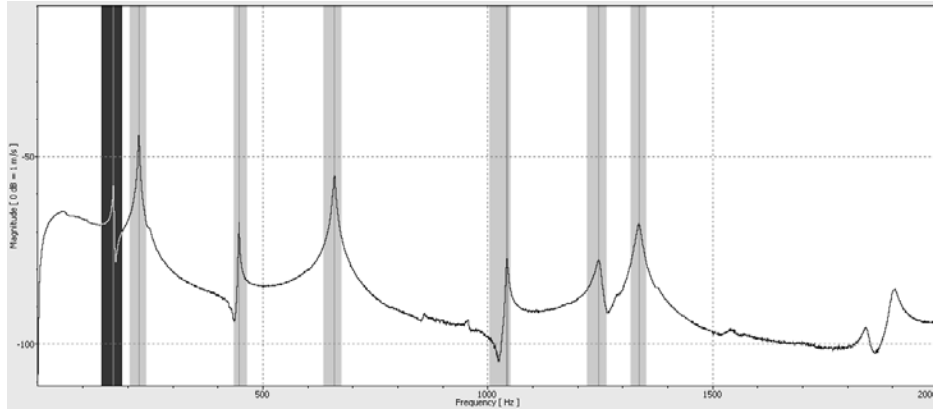


Fig. 3. Exemplary FRF and peaks selection

Rys. 3. Przykładowa funkcja odpowiedzi częstotliwościowej z zaznaczeniem pików

Table 1. Natural frequencies of the investigated specimens

Tabela 1. Częstotliwości własne drgań badanych próbek

Frequency number	Frequency, Hz			
	Undamaged	Case a	Case b	Case c
1	224.375	252.5	237.5	232.5
2	659.375	742.5	708.125	656.25
3	1336.25	1467.5	1415	1346.25

While analysing the obtained frequency values, it is possible to detect the crack presence. The evaluation of obtained values could be provided, e.g. using Modal Assurance Criterion (MAC), which shows good results in such problems [14]. However, for crack identification, methods that are more specific should be used. It will be showed in the next section using DWT.

4. Cracks identification

Signals of velocity values in defined points achieved from the experiment for selected cases were exported to the MATLAB[®] environment.

4.1. Selection of the analysing wavelet

Obtained signals for cracked beams contain some singularities, this provides information about crack location and depth. However, these singularities were not visible in signal realisations. Therefore, we use DWT to decompose the signals to approximation coefficients, which illustrates the smooth curve, and the detail coefficients, containing useful information about singularities, and this can be used for cracks identification.

The selection of the appropriate wavelet for such problems depends on several factors. The analysing wavelet must be orthogonal. The second criterion concerns some kind of compromise between the length of the effective support and the number of vanishing moments. It is necessary to select the wavelet with maximum possible number of vanishing moments and the shortest possible effective support, which assures stability and higher coefficients in damaged regions. Douka *et al.* [4, 5] used the fourth order symmetrical wavelet (*sym4*) (same as the authors of [16]) and in their further work [15], they select another two wavelets besides *sym4*: *coiflet 2* (*coif2*) and biorthogonal 6.8 wavelet (*bior6.8*). The authors of [17] used biorthogonal 5.5 wavelet (*bior5.5*) for this procedure. In the previous author's works [11], the effectiveness of the B-spline wavelets in comparison with other compactly supported orthogonal wavelets was demonstrated using the Degree of Scalogram Density. In [11], the six-order B-spline wavelet was used.

An additional parameter, which may influence crack detection effectiveness, is the number of measuring points. The authors of [15] and [16] used for the analysis 1001 and 601 measuring points, respectively. In present work, we used only 40 measuring points, which implies the necessity of applying the wavelet with shorter effective support and a sufficiently large number of vanishing moments. After some testing, the quadratic B-spline wavelet (*bsp3*) was chosen for the further analysis throughout the present work. The above-presented wavelets has four (*sym4*, *coif2*) or five (*bior5.5*, *bior6.8*) vanishing moments, but their effective supports are sufficiently large: *sym4* – 7, *coif2* and *bior5.5* – 11, *bior6.8* – 13. The chosen wavelet has 4 vanishing moments and the effective support length of 5.

4.2. Determination of the threshold for details coefficients de-noising

Considering measurement noise and disturbances induced by the wavelet, it is necessary to de-noise detail coefficients obtained from the DWT procedure for a clear detection and location of the cracks. The most used methods for de-noising are the soft- and hard-thresholding. Soft-thresholding is proposed considering its nice mathematical properties. The general procedure of de-noising consists of three steps: firstly, we decompose the signal, then we threshold detail coefficients, and finally we reconstruct the signal after the thresholding. In other words, only the detail coefficients greater than threshold

are considered. Authors of [4] used the thresholding for de-noising the detail coefficients; however, they assumed some value of threshold without explanation about its determination. Zhong and Oyadiji [15] proposed the most effective method of the thresholding yielding minimax performance multiplied by the small factor proportional to logarithmized signal length. This method could be slightly improved using a combination of the above-discussed rule and the rule based on the Stein's Unbiased Risk Estimate (SURE). Such a combination is useful when the signal-to-noise ratio is very small, and should be used when there is no opportunity to achieve the response of the undamaged structure. However, this method is based on the stochastic formulation.

In the situation when we could determine the detail coefficients for the undamaged structure, it is suitable to determine the threshold using the peak values of these coefficients. The thresholds were determined both based on statistical method and based on experimental results. Obtained thresholds are tabulated in Table 2.

Table 2. De-noising thresholds for detail coefficients
Tabela 2. Progi filtracji szumu dla współczynników detali

Case	Mode number	Method	
		Statistical (log+SURE)	Experimental
a	1	$2.5042 \cdot 10^{-6}$	$2.2680 \cdot 10^{-6}$
b	1	$2.4809 \cdot 10^{-6}$	
c	1	$2.5625 \cdot 10^{-6}$	
a	2	$2.3811 \cdot 10^{-6}$	$2.2293 \cdot 10^{-6}$
b	2	$2.4685 \cdot 10^{-6}$	
c	2	$2.2414 \cdot 10^{-6}$	
a	3	$2.5448 \cdot 10^{-6}$	$2.3951 \cdot 10^{-6}$
b	3	$2.5631 \cdot 10^{-6}$	
c	3	$2.5415 \cdot 10^{-6}$	

It is noticed that thresholds determined theoretically are slightly higher than experimentally determined. However, de-noising of detail coefficients, using both methods gives almost identical results.

4.3. Cracks detection and localisation

The procedure of cracks detection and localisation is based on DWT and IDWT. Here, the following algorithm was used: measured velocity signal was decomposed on a single-level to approximation coefficients and details coefficients; then, de-noising of obtained detail coefficients was performed using soft thresholding, and finally the reconstruction was applied only for de-noised detail coefficients. The scheme of the above-presented procedure is presented in Fig. 4. Blocks 'g' and 'h' denote low-pass and high-pass filters, respectively.

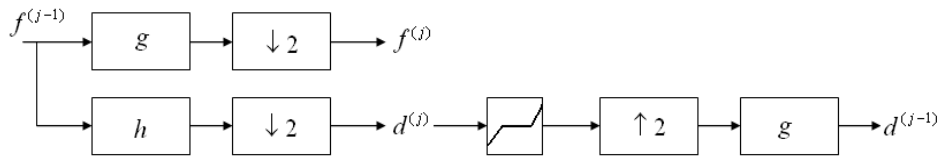


Fig. 4. Scheme of signal processing for crack detection and localisation
 Rys. 4. Schemat przetwarzania sygnału dla detekcji i lokalizacji pęknięcia

After using this procedure, the evaluation of crack position was performed. In the obtained local disturbances, the peak value indicates the crack presence. Results of the analysis are shown in Fig. 5.

It should be noted that the peak values do not reflect the crack locations in some cases (e.g. Fig. 5, Case a, Mode 2). In this case, the effect of the sign of detail coefficients appeared. In the some region, where detail coefficients are negative, we could observe a mirror image position of the true crack location [18]. Following this, the true crack position could be determined as a difference of the L_{eff} and pseudo-crack position. In the presented results, the above-mentioned effect could be observed for Case b Mode 2 and Case c Mode 3.

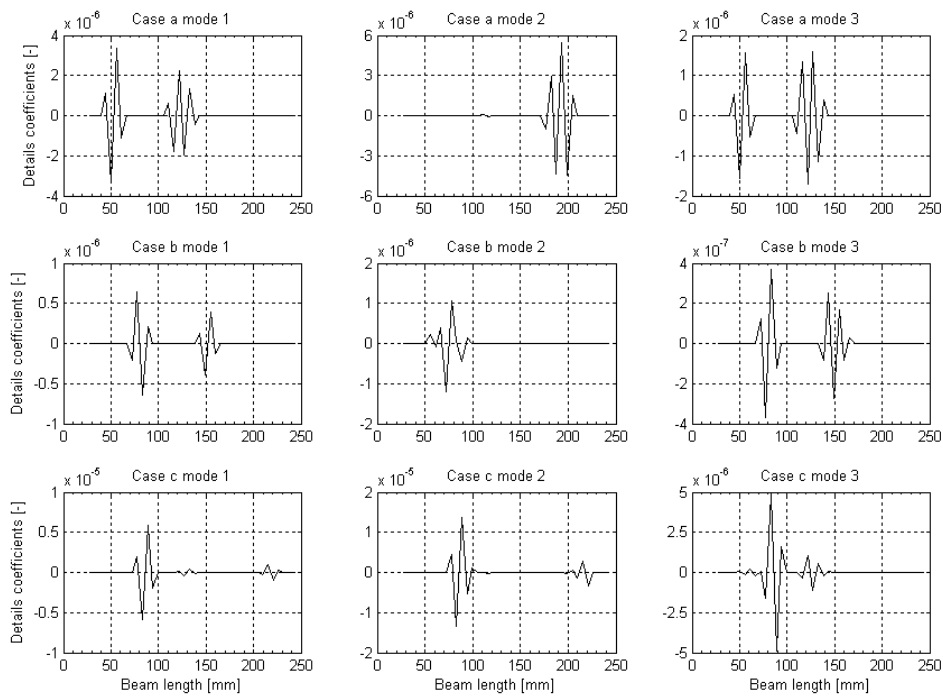


Fig. 5. Results of cracks detection and localization procedure
 Rys. 5. Wyniki procedury detekcji i lokalizacji pęknięć

4.4. Discussion on the estimation of cracks depth

The problem of the crack depth estimation using wavelet transform has been discussed by many authors, e.g. [4, 16]. Douka *et al.* in [4, 5] proposed the crack depth estimation using the relative differences observed in the detail coefficients set. They established the intensity factor based on the modal model of a cracked beam. Zhong and Oyadiji in [16] used a similar method and also discussed the influence of crack depth on the sign of detail coefficients. Both of above-presented methods are based upon the comparative analysis of detail coefficients of cracked beams with various crack depths. Such an approach allows the estimation of cracks depth only as a relative one and does not give the depth value explicitly.

The problem of crack depth estimation becomes very complicated, taking into consideration following effects. First, the relation between the crack position and the actual modal shape must be considered. Let us analyse the results in Fig. 5 for Case a. For the first mode, it could be observed that first absolute local peak value is greater than the second one, which confirm the actual state (see Fig. 1). However, for the second mode, we obtain different result: the detail coefficients in the first crack location have great magnitude, but the second one is almost undetectable. This is reasoned by the mode shape: the second crack is located very close to the modal node; thus, the magnitude of the detail coefficients in this location is quite low. For the third mode, we obtain almost identical magnitudes of local peaks of detail coefficients, but originally their depths differ by a factor of two. The influence of modal shape is clearly visible for Case b Mode 1. The beam contains two cracks with different locations but with the same crack depth; however, local peaks of detail coefficients on Fig. 5 show recognisable differences.

Summarising, at the present time, there is no effective method for the explicit estimation of crack depth. The crack depth could be evaluated using the mixed theoretical-experimental approach, but this method will be limited to simple geometrical cases due to the complexity of theoretical modelling of real structural components.

5. Conclusions

The paper considers the problem of multiple crack identification in polymeric laminate beams using DWT. The modal responses of damaged beams were obtained using laser Doppler vibrometer for first three modal shapes. Measured signal realisations, as expected, contain two types of noise: an experimental and wavelet disturbance. Therefore, it was necessary to investigate two subsidiary problems: the selection of the appropriate wavelet for effective crack recognition and simultaneously minimising local disturbances; and the selection of the appropriate method for detail coefficients de-noising.

Comparative analyses and discussions on these problems were performed. Using optimal wavelet and de-noising procedures, the signal processing was carried out using a modified method. After signal decomposition, one considers only details coefficients, which were de-noised and reconstructed. The proposed algorithm gives good results, i.e. we detect and localise all of the cracks in each investigated specimen. Several useful aspects, like the effect of the sign of detail coefficients and the influence of the modal shape on detail coefficient magnitudes, were also discussed. The proposed method has a few limitations. First of all, it can be used only for the transverse crack identification during bending excitation, and the accuracy of the method is strongly influenced by the type of applied wavelet, the sampling distance, and the number of measuring points. However, the method could be applied in a large group of industrial applications, which fulfil the above criteria.

References

- [1] Ghoneam S.M., Dynamic analysis of open cracked laminated composite beams, *Composite Structures*, 32, pp. 3–11, 1995.
- [2] Abd El-Hamid Amada A., An investigation into the eigen-nature of cracked composite beams, *Composite Structures*, 38, pp. 45–55, 1997.
- [3] Katunin A., Moczulski W., Faults detection in layered composite structures using wavelet transform, *Diagnostyka* 1(53), pp. 27–32, 2010.
- [4] Douka E., Loutridis S., Trochidis A., Crack identification in beams using wavelet analysis, *International Journal of Solids and Structures*, 40, pp. 3557–3569, 2003.
- [5] Loutridis S., Douka E., Trochidis A., Crack identification in double-cracked beams using wavelet analysis, *Journal of Sound and Vibration*, 277, pp. 1025–1039, 2004.
- [6] Grabowska J., Palacz M., Krawczuk M., Damage identification by wavelet analysis, *Mechanical Systems and Signal Processing*, 22, pp. 1623–1635, 2008.
- [7] Rucka M., Wilde K., Crack identification using wavelets on experimental static deflection profiles, *Engineering Structures*, 28, pp. 279–288, 2006.
- [8] Tian J., Li Z., Su X., Crack detection in beams by wavelet analysis of transient flexural waves, *Journal of Sound and Vibration* 261, pp. 715–727, 2003.
- [9] Sekhar A.S., Multiple cracks effects and identification, *Mechanical Systems and Signal Processing*, 22, pp. 845–878, 2008.
- [10] Katunin A., Korczak A., The possibility of application of B-spline family wavelets in diagnostic signal processing, *Acta Mechanica et Automatica*, 3(4), pp. 43–48, 2009.
- [11] Katunin A., Construction of high-order B-spline wavelets and their decomposition relations for faults detection and localization in composite beams, *Acta Mechanica et Automatica*, 2010, submitted.
- [12] Mallat S., A theory of multiresolution signal decomposition: the wavelet representation, *IEEE Trans. Patt. Anal. Mach. Intel.*, 11, pp. 674–693, 1989.
- [13] Katunin A., Moczulski W., The conception of a methodology of degradation degree evaluation in laminates, *Maintenance and Reliability*, 1(41), pp. 33–38, 2009.
- [14] Deraemaeker A., Preumont A., Vibration based damage detection using large array sensors and spatial filters, *Mechanical Systems and Signal Processing*, 20, pp. 1615–1630, 2006.
- [15] Douka E., Loutridis S., Trochidis A., Crack identification in plates using wavelet analysis, *Journal of Sound and Vibration*, 270, pp. 279–295, 2004.

- [16] Zhong S., Oyadiji S.O., Crack detection in simply supported beams using stationary wavelet transform of modal data, *Structural Control and Health Monitoring*, 2010, early view.
- [17] Rucka M., Wilde K., Application of continuous wavelet transform in vibration based damage detection method for beams and plates, *Journal of Sound and Vibration*, 297, pp. 536–550, 2006.
- [18] Zhong S., Oyadiji S.O., Crack detection in simply supported beams without baseline modal parameters by stationary wavelet transform, *Mechanical Systems and Signal Processing*, 21, pp. 1853–1884, 2006.

Manuscript received by Editorial Board, July 27th 2010

Identyfikacja wielopółożeniowych pęknięć w belkach kompozytowych z zastosowaniem dyskretnej transformacji falkowej

Streszczenie

W pracy przedstawiono metodę identyfikacji pęknięć wielopółożeniowych opartą o dyskretną transformację falkową. Analiza została przeprowadzona na belkach z laminatu polimerowego. Wyznaczenie lokalizacji pęknięć polegało na ocenie postaci własnych drgań belek z pęknięciami. Postacie własne były otrzymane eksperymentalnie za pomocą dopplerowskiej wibrometrii laserowej. Odpowiedź dynamiczna belek z pęknięciami była przetworzona z zastosowaniem dyskretnej transformacji falkowej, a następnie rozpatrzono współczynniki detali w celu identyfikacji pęknięć. Dalej omówiono metody usuwania szumu ze współczynników detali. Zbadano kryteria wyboru odpowiednich falek. Zaproponowana metoda wykazała efektywność w identyfikacji pęknięć wielopółożeniowych i może być z powodzeniem zastosowana w rozwiązaniach przemysłowych kontroli stanu struktur.

LESZEK KNOPIK*

Mixture of distributions as a lifetime distribution of a technical object

Key words

Failures, failure rate function, mixture of distributions.

Słowa kluczowe

Uszkodzenia, funkcja intensywności uszkodzeń, mieszanina rozkładów.

Summary

The lifetime distribution is very important in reliability studies. The shape of lifetime distribution can vary considerably; therefore, it frequently cannot be approximated by simple distribution functions. This article is connected with the problem of finding of lifetime distribution with a unimodal failure rate function. For this purpose, the mixture of two distributions has been considered.

We show that a unimodal failure rate function can be obtained as a failure rate function of the mixture of an exponential and Rayleigh distributions. The numerical examples are also provided to illustrate the practical impact of this approach.

* University of Technology and Life Science, Bydgoszcz, Department of Applied Mathematics, Kaliskiego st. 7, 85-789 Bydgoszcz, Poland, phone 52 340 8208, e-mail: knopikl@utp.edu.pl.

1. Introduction

An important topic in the field of lifetime data analysis is to select the most appropriate lifetime distribution. This distribution describes the time to failure of a component, subsystem, or system. Some number of the failures are results from natural wear of the machines, while other failures may be caused by inefficient repair of the previous failures. They result from incorrect organisation of the repairs. The analysis of the results of the operation and maintenance investigations regarding the moments the failures occur prove that the set of the failures may be divided into two subsets of the primary and secondary failures. The population of times to failure is heterogeneous. The resulting population of lifetimes can be described using the statistical concept of a mixture.

The analysis of the empirical data (the length of the time intervals between the failures) indicates that it is reasonable to describe the probability distribution of the correct work times with density function $f(t)$ as follows:

$$f(t) = p \lambda e^{-\lambda t} + (1 - p) f_2(t) \quad (1)$$

where $\lambda > 0$, $0 < p < 1$ and $f_2(t)$ is unknown density. This model was proposed in paper [17]. The density $f(t)$ is a mixture of an exponential distribution and a distribution with density function $f_2(t)$.

In this paper, we study the mixture of an exponential distribution and a Rayleigh distribution. A purpose of this paper is construction of a mixture of distribution with an unimodal failure rate function. The distribution with a non-monotonic failure rate function is considered in reliability theory. The distribution with a bathtub shaped failure function (BFR) belongs to such a situation. In reliability theory, the models with BFR are very useful. A brief discussion and summary for such a distribution is given in [4] and [14]. However, there are many known examples of the application of distribution with upside-down bathtub shaped (unimodal) failure rate function (UBFR). In a particular case, the unimodal failure rate function is used in [15] and [16] to analyse the lifetime of a biological population, [1] medical data, [12] data of motor bus failure, [4] and [6] optimal burn decision, [10] ageing property in reliability, and [2] social mobility. One way of generating a distribution with a non-monotone failure rate function is the mixing of standard distributions. It is commonly known that a mixture of distributions with a decreasing failure rate function (DFR) has a decreasing failure rate function (Prochan [13]). In [9], there has been given the condition under which the mixture of an exponential distribution and an IFR (increasing failure rate function) is a DFR distribution.

Mixture gamma distribution and exponential distribution studies are shown in [7]. Klutke et al. [11] has studied the mixture of Weibull distributions and suggest that the this mixture can be a distribution with a unimodal failure rate function. However, in [19], the failure rate function has a decreasing initial period. The mixture of the two Weibull distributions has been studied in [18]. The same values of the scale parameter have given all possible types of shape failure rate functions and, for the different scale parameters, numerical computing is performed. Block et al. [5] has studied the mixture of two distributions with increasing linear failure rate functions.

Section 2 concerns a model of the mixture of distributions. In Section 3, we consider numerical examples with technical data.

2. The model of mixture distributions

We consider a mixture of the lifetimes T_1 and T_2 with the densities $f_1(t)$, $f_2(t)$, the reliability functions $R_1(t)$, $R_2(t)$, the failure rate functions $\lambda_1(t)$, $\lambda_2(t)$ and weights p and $1 - p$, where $0 < p < 1$. The mixed density function is then written as

$$f(t) = p f_1(t) + (1 - p) f_2(t)$$

and the reliability function is

$$R(t) = p R_1(t) + (1 - p) R_2(t)$$

The failure rate function of mixture can be written as the mixture [3]

$$\lambda(t) = w(t) \lambda_1(t) + (1 - w(t)) \lambda_2(t)$$

where $w(t) = p R_1(t)/R(t)$. Moreover, from [3], we have, under some mild conditions, that

$$\lim_{t \rightarrow \infty} \lambda(t) = \lim_{t \rightarrow \infty} \min\{\lambda_1(t), \lambda_2(t)\}$$

In the following proposition, we give properties for the failure rate function of mixture.

Proposition 1: For the first derivative of $w(t)$, we have

$$w'(t) = w(t) (1 - w(t)) (\lambda_2(t) - \lambda_1(t))$$

Proposition 2: For the first derivative of $\lambda(t)$, we obtain

$$\lambda'(t) = (1 - w(t)) (-w(t) (\lambda_2(t) - \lambda_1(t))^2 + \lambda_2'(t)) + w(t) \lambda_1'(t)$$

Proposition 3: If $R_1(t) = \exp(-\lambda_1 t)$, for $t \geq 0$, then

$$\lambda'(t) = (1 - w(t)) (-w(t) (\lambda_2(t) - \lambda_1)^2 + \lambda_2'(t))$$

Let $\lambda_1(t) = \lambda$, $\lambda_2(t) = at + b$, where $a > 0$, $b \geq 0$. The cumulative failure rate function is

$$\Lambda_2(t) = \frac{1}{2} a t^2 + b t$$

and the reliability function

$$R_2(t) = \exp\{-\frac{1}{2} a t^2 - b t\}$$

Let $h_1(t) = \lambda_2'(t) = a$, $h_2(t) = w(t) (\lambda_2(t) - \lambda)^2$. We will consider two cases: $\lambda \leq b$ and $\lambda > b$.

Case A: $\lambda \leq b$.

In this case the function $h_2(t)$ is increasing from $h_2(0) = p(b - \lambda)^2$ to ∞ . If $a \leq p(b - \lambda)^2$ then $h_2(t) > h_1(t)$, and $\lambda'(t) < 0$. In this case $T \in \text{DFR}$.

If $a > p(b - \lambda)^2$ then the equation $h_2(t) = h_1(t)$ has one solution. In this case, the failure rate $\lambda(t)$ is unimodal.

Case B: $\lambda > b$.

In this case, there is $t_1 = (\lambda - b)/a$ such that $h_2(t_1) = 0$. The function $h_2(t)$ is decreasing on $(0, t_1)$, and increasing on (t_1, ∞) . If $p(b - \lambda)^2 \geq a$, then the equation $h_2(t) = h_1(t)$ has exactly one solution t_2 such that $t_2 > t_1$. Hence, $\lambda(t)$ is unimodal.

If $p(b - \lambda)^2 < a$, then the equation $h_2(t) = h_1(t)$ has exactly two solutions t_3 and t_4 such that $0 < t_3 < t_1$ and $t_1 < t_4$. In this case the failure rate function $\lambda(t)$ of the mixture is decreasing on $(0, t_3)$, increasing on (t_3, t_4) , and decreasing on (t_4, ∞) . This failure rate function we describe as a modified unimodal. We showed the following:

Proposition 4: If $b - \sqrt{\frac{a}{p}} < \lambda \leq b$ or $\lambda \geq b + \sqrt{\frac{a}{p}}$ then the failure rate

function $\lambda(t)$ of the mixture (1) is unimodal.

3. Numerical examples

In this section, numerical examples are given to illustrate this model.

Example 1. We assume that $a = 0.5$, $b = 1$, $\lambda = 2$, $p \in \{0.125, 0.25, 0.375, 0.5, 0.625\}$. Fig. 1 shows a graphics of the failure rate function for this example. For $p = 0.625$, we have the modified unimodal failure rate function and for remaining values of p unimodal shape.

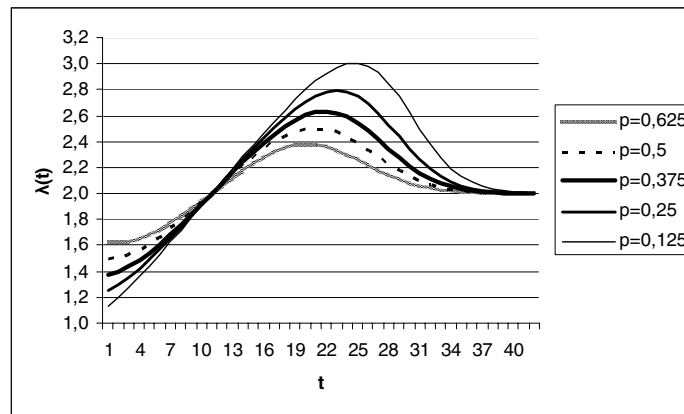


Fig. 1. The failure rate function for Example 1
Rys. 1. Funkcja intensywności dla przykładu 1

Example 2. In this example, we consider a real lifetime data. The object of the investigation is a real municipal bus transport system within a large agglomeration. The analysed system operates and maintains 210 municipal buses of various manufacturers and types. For investigation purposes, 35 buses of the same make were selected. The data set contains $n = 2700$ times between successive failures of the electrical system of the bus.

By maximising the logarithm of the likelihood function for grouped data, we have estimated the values of the parameters a , b , λ and p of the reliability function

$$R(t; a, b, \lambda, p) = p \lambda \exp(-\lambda t) + (1 - p) \exp(-0.5 a t^2 - b t) \quad (2)$$

Values of these parameters are the following: $a = 3.6476$, $b = 0.4495$, $\lambda = 0.06813$, $p = 0.6756$.

We prove Kolmogorow's test of fit and compute the associated p -value, p -value = 0.14. The reliability function (2) sufficiently and precisely describes the empirical reliability function. Fig. 2 shows the failure rate function for Example 2.

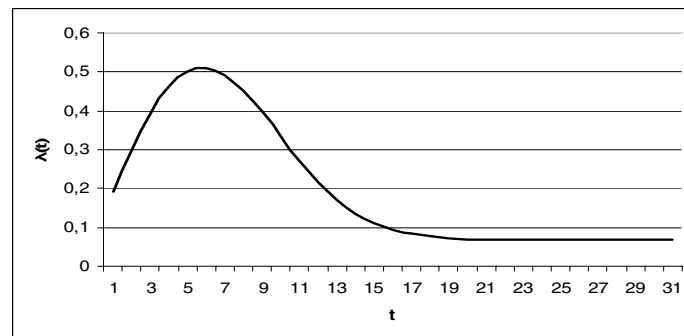


Fig. 2. The failure rate function for Example 2
Rys. 2. Funkcja intensywności dla przykładu 2

4. Conclusions

The basic idea discussed in this article is the application of the mixture of two standard distributions. In this paper, we study and attempt to determine the shape as well as the overall behaviour of the failure rate function of a mixture from two subpopulations, the exponential and Rayleigh distributions. This mixture can be used for the construction of the lifetime distribution of a technical object. The numerical example for the lifetime of an electrical system of a bus shows that a mixture can be useful for practical applications.

References

- [1] Aalen O.O., Gjessing H.K.: Understanding the shape of hazard rate: a process point view, *Statistical Science*. 2001,16, pp. 1–22.
- [2] Allison P.D.: *Event History Analysis*, Sage, 1984.
- [3] Block H.W., Joe H.: Tail behavior of the failure rate function of mixtures, *Lifetime Data Analysis*, 1997, 3, pp. 269–288.
- [4] Block H.W., Savits T.H.: Burn-in, *Statistical Science* 1997, 12, 1–13.
- [5] Block H.W., Savits T.H., Wondmagegnehu E.T.: Mixtures of distributions with increasing linear failure rates. *Journal Application Probability*, 2003, 40, pp. 485–504.
- [6] Chang D.S.: Optimal burn – in decision for products with an unimodal failure rate function, *European J. Oper. Res.* 2000, 126, pp. 584–640.
- [7] Gleser L.J.: The gamma distribution as a mixture of exponential distributions. *American Statistics*, 1989, 43, pp. 115–117.
- [8] Gupta G.L., Gupta R.C.: Ageing characteristics of the Weibull mixtures, *Probability in the Engineering and Information Science*, 1996, 10, pp. 591–600.
- [9] Gurland J., Sethuraman I.: How pooling failure data may reverse increasing failure rates when pooling failure data, *Technometrics*, 1984, 36, pp. 416–418.
- [10] Jiang R., Ji P., Xiao X.: Ageing property of unimodal failure rate models, *Reliability Eng. System Safety*, 2003, 79, pp. 113–116.
- [11] Klutke G.A., Kiessler P.C., Wortman M.A.: A critical look at the bathtub curve, *IEEE Transaction on Reliability*, 2003, 54, pp. 125–129.
- [12] Mudholkar G.S., Srivastava D.K., Feimer M.: The exponentiated Weibull family: a reanalysis of the bus–motor failure data, *Technometrics*, 1995, 37, pp. 436–475.
- [13] Proschan F.: Theoretical explanation of observed decreasing failure rate, *Technometrics* 1963, 5, pp. 375–383.
- [14] Rajarschi S., Rajarshi M.B.: Bathtub distributions: A review. *Comm. Statist.* 1988, 17, pp. 2597–2621.
- [15] Vaupel J.W., Yashin A.I.: Some surprising effects of selection on population dynamics, *American Statistics*, 1985, 39, pp. 176–184.
- [16] Wang J., Muller H., Capra W.B.: Analysis of oldest–old morality: lifetimes revisited, *Annals Statistic*, 1998, 26, pp. 126–133.
- [17] Wdzięczny W., Woropay M., Muślewski Ł.: Division and investigation of damages to technical objects and their influence on the reliability of operations of complex operation and maintenance systems. *Scientific Problems of Machines Operation and Maintenance 2* (154), 2008, pp. 31–43.
- [18] Wondmagegnehu E.T.: On the Behavior and shape of Mixture Failure Rate Family of IFR Weibull Distributions, *Naval Research Logistics*, 2004, 51, pp. 491–500.

- [19] Wondmagegnehu E.T., Nawarro J., Hernandez P.J.: Bathtub Shaped Failure Rate From Mixture: A practical Point of View, IEEE Transaction on Reliability, 2005, 54, pp. 270–276.

Manuscript received by Editorial Board, September 8th 2010

Mieszana rozkładów jako rozkład czasów życia obiektu technicznego

Streszczenie

Rozkłady czasów życia są bardzo ważne w badaniach niezawodnościowych. Kształt dystrybuanty czasu życia można badać dokładnie i wtedy często nie można go aproksymować przez proste rozkłady.

Pokazujemy, że jednomodalną funkcję intensywności uszkodzeń można otrzymać jako funkcję intensywności uszkodzeń mieszaniny rozkładu wykładniczego i rozkładu Rayleigha. W celu pokazania praktycznego znaczenia tego podejścia podano przykłady numeryczne.

MAŁGORZATA WRONA*

**The application of the computer image analysis
in wear particle research**

Key words

Wear mechanisms; wear particle analysis, lubricating oils, computer image analysis.

Słowa kluczowe

Mechanizmy zużywania, analiza cząstek zużycia, oleje smarowe, komputerowa analiza obrazu.

Summary

In this research, the possibilities of characterising the texture, colour and contour of wear particles were investigated. The assessment of the texture and colour of wear particles on the basis of the analysis of changes in the grey-scale and individual components of the colour model CIE L*a*b* was performed. For a statistical description of distributions, the following parameters were used: the averages grey-level and the values of maximal and minimal grey-level. The assessment of the surface texture and contour of wear particles by the Fourier and fractal analyses was also carried out. The amplitude spectrum numerical parameters for chosen lines marked on the particle image were determined with the help of one dimension Fast Fourier Transformation (FFT). Based on the suitably prepared data obtained from images, the fractal dimension of the contour of the investigated particles, using the compass method, was determined. The usefulness of the determined parameters was evaluated by determining the wear particles' affiliation to the suitable

* Institute for Sustainable Technologies, National Research Institute, 26-600 Radom, Pułaskiego 6/10, Poland, phone (48) 361-42-41.

type. The correlation between morphological features of wear particles and mechanisms taking place during friction couple wear was determined on the basis of an analysis of the obtained research results of individual groups of wear particles.

1. Introduction

As the result of the operation of the tribological processes taking place in friction couples of machines and devices, the wear products, being metal particles or their oxides, appear. The features and quantities of these products are determined by the properties of the surface layers of the cooperating tribological elements, exploitation conditions, the quality of the lubricating substance, and its tribological properties. Empirical correlation between different features of wear particles and wear mechanisms can be used as basis for the identification of particle types and the determination of the wear mechanism, providing an assessment of the state of friction couples [1]. The application of computer image analysis enables conducting the comprehensive assessment of wear particles on which it is possible to base friction couple diagnosis [1-13].

The aim of work was to determinate the morphological features of wear particles obtained in laboratory tribological tests.

2. Materials and methods

For the purpose of obtaining the particles, the tribological testers, prod. ITeE – PIB in Radom were applied [14]. The construction of the friction couples and their conditions of movement were taken into consideration in choosing the testers. The tests were conducted under conditions of adhesive, scuffing, abrasive, and fatigue wear.

Tests of adhesive and abrasive wear were performed using the apparatus T-01 M. The pin with 3 mm diameter was made of LH 15 steel, having a hardness of 60 HRC. The disc with a 45 mm diameter was made of 45 steel, having a hardness of 30 HRC. Three different loads 10, 30, and 50 N, were employed, the sliding speed used was 0.5 m/s, and the friction distance was 500 m. The test lasted 1000 s.

For the conducting of fatigue wear test (under oscillatory sliding conditions) the apparatus T-19 was used. The disc used for the test was 25 mm in diameter and the ball was 10 mm in diameter. Both the disc and ball were made of LH 15 steel with a hardness of 60 HRC. The test parameters were as follows: loads 50 and 100 N, the amplitude of movement = 0.6 mm, and the frequency of oscillation = 50 Hz. Friction was performed under unlubricated conditions. The test was 10 min in duration.

The scuffing wear test was carried out using a four-ball tester T – 02 in accordance with standard PN–76/C–04147. It involved conducting 10–second runs of the set of four balls under a gradually increasing load in presence of an investigated lubrication product until welding signs occurred. In the test, ½" diameter steel balls of hardness 60 HRC and surface roughness of 0.32 µm (R_a) were used, and the lubricant was SN 400 base oil.

Preparation of the particles provided involved isolating them from the lubrication medium through ultrasonic rinsing and filtration for research.

The wear particles images were recorded and stored for further analyses with the use of a commercial system of computer image processing and analysis - Computer Scanning Systems Ltd. prod. Poland equipped with the following:

- MM-40 microscope model L3FA prod. Nikon;
- A digital optical camera, Industrial Colour CCD Camera, model GP-KR222E prod. Panasonic;
- Indeo fast Frame Grabber card; and
- IBM PC class computer with Pentium processor, Windows XP operating system and software for analysis of microscopy images Multiscan v. 14.02.

The source of light in the light microscope was a halogen light bulb giving a colour temperature around 3000 °C. The images were recorded using reflected light illumination for revealing the details of their surface and colour. To improve the depth of sharpness, the images were registered with a partially closed diaphragm. The reduction of reflection was achieved through the possibility of the adjustment of the setup of the diaphragm. The image magnifications used during registration were 500, 200 and 50, depending on the size of the particles. For conducting measurements, the system was defined and calibrated according to model image and measurement unit.

For the research of images with the use of colour model L*a*b*, one of several known programs was chosen for graphic processing of the bitmap images with Adobe Photoshop. This program offers the possibility of displaying a histogram of the distribution of grey-scales in individual colour channels and the global grey-scale for a given area. It allows one to perform measurements on registered digital images; therefore, it realises some tasks of digital image analysis. The histogram window presents the distributions of component colours, which are not standard values. Transformation of data is possible according to the following formulas:

$$L^* = \frac{L}{255} \times 100 \quad (1)$$

$$a^* = \frac{240a}{255} - 120 \quad (2)$$

$$b^* = \frac{240b}{255} - 120 \quad (3)$$

Where:

- L, a, b – components displayed in histogram window with values from 0 to 255,
- L^* – achromatic component normalised to the range (0, 100), contains information concerning image luminance,
- a^* – chromatic component normalised to the range (-120, 120), contains information about colours from green to red,
- b^* – chromatic component normalised to the range (-120, 120), contains information about colours from blue to yellow.

The one dimensional Fast Fourier Transformation (FFT) contained in the Multiscan program was used for the realisation of texture analysis. The texture research of wear particles was performed by carrying out Fourier analysis for points of chosen lines marked on the particle image. The positions and lengths of the measuring lines were dependent on the dimensions and shapes of investigated particles. In order to assure the comparability of results for all particles, the same number of elements of input series n equal to 32 was accepted. Results of successive measurements were recorded in text files for utilisation in further analyses.

For analysis of contour algorithm contained, the program Multiscan was used. Fractal dimensions of the contours of investigated particles were obtained by using the chord method. Fractal analysis of particles involved the replacement of their contour by a broken line with apexes tangent to a contour and constant length side. The procedure was repeated for all chosen lengths of a side. Calculated values were the basis for plotting the dependence of the logarithm of the broken length from the logarithm of length of the side in the form of a linear regression equation.

In conducting the research, the number of analysed images of individual types of particles was 10 or 5, depending on method of research. This number of particles was necessary to obtain a useful result during the simultaneous limitation of times of the research.

3. Discussion of research results

The research included the assessment of the colours, textures, and contours of wear particles. As a result of the analysis of the series of particles, related to the components in the CIE $L^*a^*b^*$ colour model, Fourier coefficients and fractal dimension were determined.

4. L^* , a^* , b^* colour components

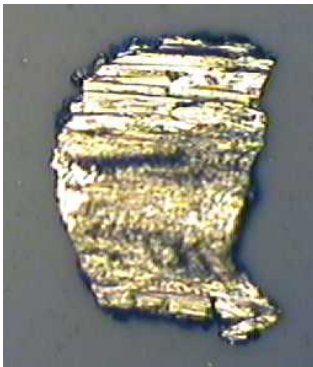
The results of the colour analysis of the investigated wear particles in the CIE $L^*a^*b^*$ system are presented in Table 1. Data concern 10 particles of each kind. The analysis the colours of wear particles indicated differences in the brightness of individual types of particles. Each type of particle is represented on a histogram (Figs. 1 and 2) by bands placed in certain characteristic areas of the changes of lightness, which allows for their classification. The lowest values of lightness were found for the following wear particles: adhesion under load of 10 N, abrasion and scuffing under load of 1000 N ($L^* = 34.41, 40.59$ and 40.64 , respectively). The highest values were for the following wear particles: scuffing under load of 500 N and adhesion under load of 30 N ($L^* = 63.78$ and 57.13 , respectively). A good indicator of the differences between the investigated types of wear particles are also the values of a^* . In the case of wear particles, with scuffing under a load of 1000 N and abrasion, the average value of the a^* component was negative, indicating the presence of green colour. In all remaining cases, positive values of a^* component were found, which in turn indicates the presence of red colour. For fatigue wear particles, the numerical values of this parameter were respectively, 9.23 under load of 100 N, and 6.25 under load of 50 N, which proves a relatively high share of this colour. The range of changes of a^* values suggests that the green component was also present in other particle types. The b^* component showed negative values for adhesive, abrasive, and fatigue wear particles, while adhesive wear particles under load of 10 N ($b^* = -11.83$) were characterised by the highest degree of blue colour saturation. However, the highest saturation of yellow colour was observed for scuffing wear particles under a load of 500 N ($b^* = 8.73$). The obtained results indicate the usefulness of the $L^*a^*b^*$ model in research for the purpose of the identification of particle colours. It solves the problem of differences in colour reproduction resulting from use of various devices. Through the introduction of quantitative estimation and the elimination of subjective factors during research, the described method should lead to correct and exact identification of particle types. The other statistical parameters describing colour such as standard deviation, skewness, and kurtosis can be also subjected to estimation. When making a choice of the most effective parameters, it is possible to apply advanced methods of data analysis, e.g. PCA method.

Table 1. Average, minimal and maximal values L^* , a^* , b^* of wear particles
 Tabela 1. Wartości średnie, minimalne i maksymalne L^* , a^* , b^* cząstek zużycia

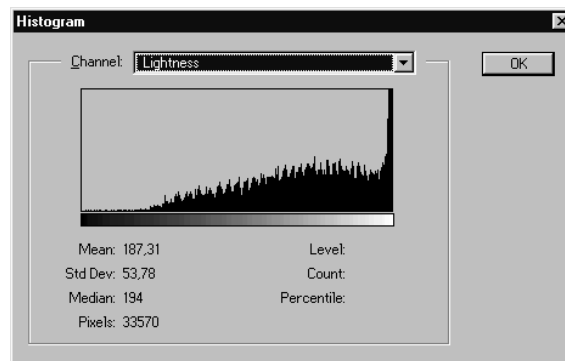
No.	Wear particles type	Statistic parameters	L^*	a^*	b^*
1.	Adhesive wear particles – load 10 N	Min. - Max.	28.18 – 49.78	-3.95 – 3.76	-17.56 – -2.46
		Average value	34.41	1.73	-11.83
2.	Adhesive wear particles – load 30 N	Min. - Max.	38.26 – 75.62	-2.55 – 2.00	-16.20 – 2.42
		Average value	57.13	0.05	-4.4
3.	Adhesive wear particles – load 50 N	Min. - Max.	31.02 – 67.74	-1.04 – 1.84	-15.98 – 5.66
		Average value	47.80	0.34	-5.71
4.	Scuffing wear particles – load 500 N	Min. - Max.	49.16 – 78.98	-1.06 – 1.67	-3.68 – 15.12
		Average value	63.78	0.02	8.73
5.	Scuffing wear particles – load 1000 N	Min. - Max.	32.95 – 65.65	-3.43 – 4.29	-5.98 – 22.83
		Average value	40.64	-1.17	0.84
6.	Abrasive wear particles – load 30 N	Min. - Max.	33.19 – 46.52	-2.73 – -0.71	-10.03 – -2.78
		Average value	40.59	-1.46	-6.12
7.	Fatigue wear particles – load 50 N	Min. - Max.	46.01 – 56.30	4.14 – 9.36	-15.40 – 0.17
		Average value	52.33	6.25	-8.5
8.	Fatigue wear particles – load 100 N	Min. - Max.	48.76 – 64.58	3.69 – 14.25	16.08 – 10.89
		Average value	54.63	9.23	-3.29

The extreme values were obtained based on 10 particles.

a)



b)



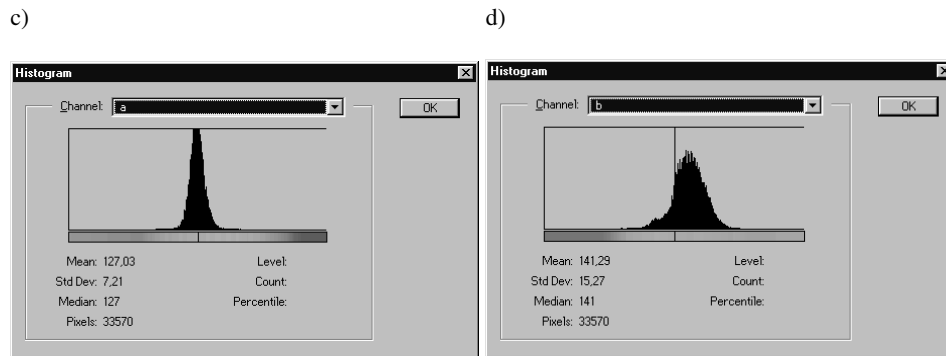


Fig. 1. Image of a scuffing wear particle under contact load of 500 N (a) and histograms of grey levels (b) and components a (c) and b (d)

Rys. 1. Obraz cząstki zużycia scuffingowego przy obciążeniu styku 500 N (a) oraz histogramy jasności (b) i składowych: a (c) i b (d)

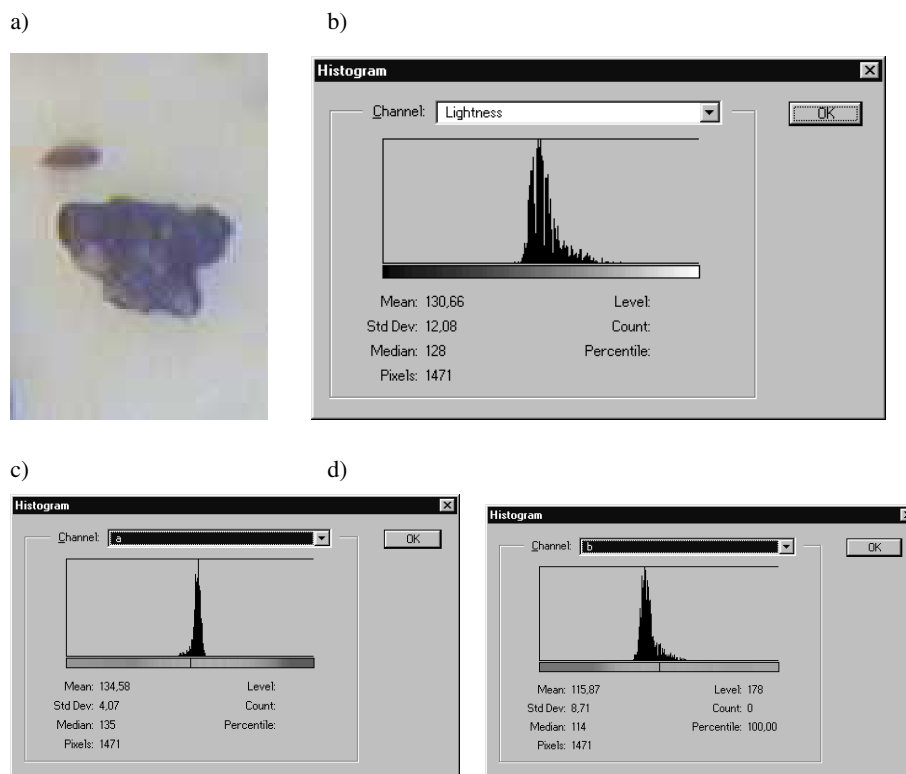


Fig. 2. Image of a fatigue wear particle under contact load of 100 N (a) and histograms of grey levels (b) and components a (c) and b (d)

Rys. 2. Obraz cząstki zużycia zmęczeniowego przy obciążeniu styku 100 N (a) oraz histogramy jasności (b) i składowych: a (c) i b (d)

5. Fourier coefficients

In Fig. 3, an example of the amplitude spectra, obtained for adhesive wear particles, is presented. On the images of these particles, segments subjected to analysis are marked by a continuous line. On the abscissae axis of the spectrum diagram are located the successive harmonic components ($n = 32$), and the ordinate's axis presents the values of spectra in the form of brightness levels from range of 0 – 255. The average values of the harmonic components for the chosen five wear particles of each kind are shown in Fig. 4 and Table 2. The number of harmonic components has been limited from 32 to 16, in which the whole or part of the spectrum power is concentrated.

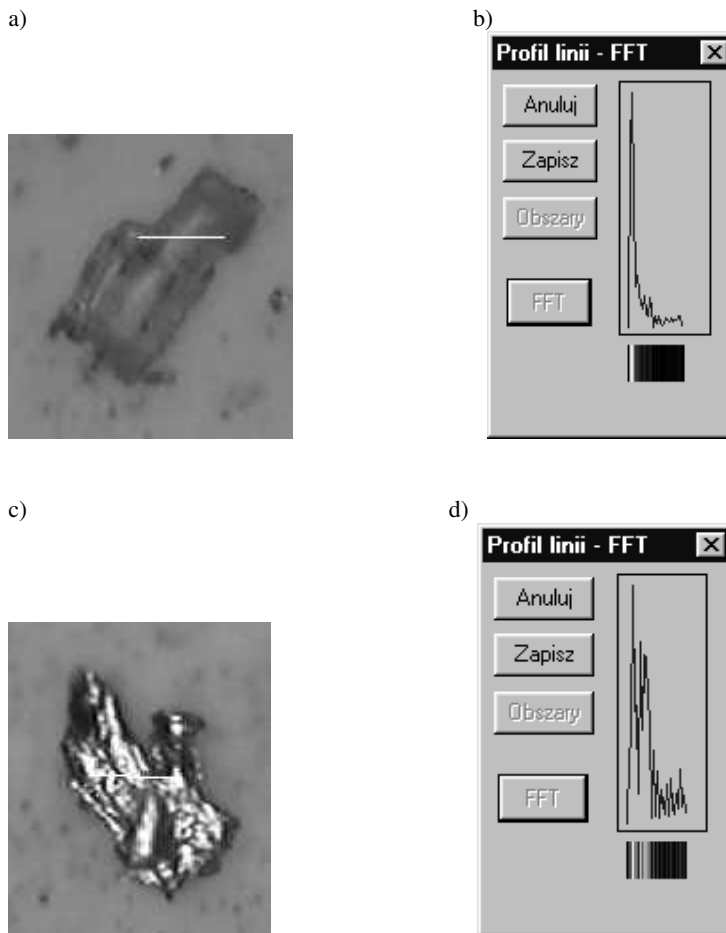


Fig. 3. Images of the adhesive wear particles under contact load of 10 (a) and 50 N (c) and correspond to them Fourier amplitude spectra (b) and (d)

Rys. 3. Obrazy cząstek zużycia adhezyjnego przy obciążeniu 10 (a) i 50N (c) i odpowiadające im fourierowskie widma amplitudowe (b) i (d)

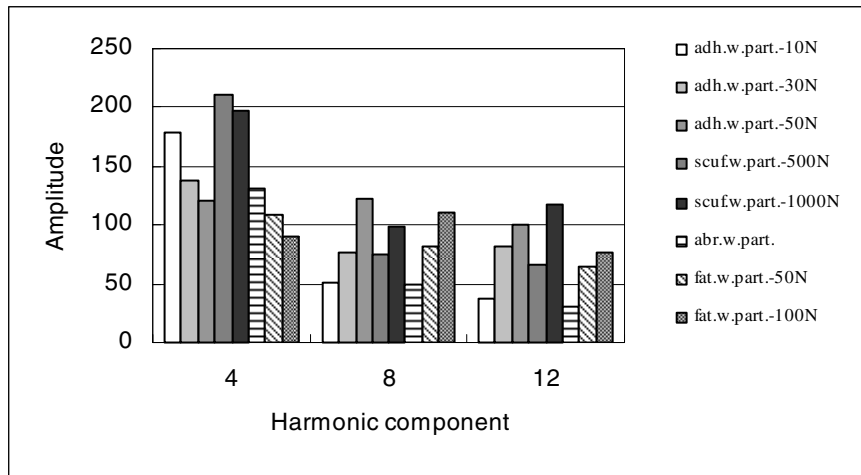


Fig. 4. The graph of the harmonic amplitudes for lines marked on the particles' surface
 Rys. 4. Wykres amplitud składowych harmoniczných odcinków zaznaczonych na powierzchni cząstek

The analysis of the harmonic components of the amplitude spectrum for chosen types of wear particles has shown that, in case wear particles, adhesion under a load of 10 N, and abrasion, the levels of second, third, and fourth harmonic component are higher than the level of other harmonics, which shows that image includes a smooth transition without violent changes in the levels of brightness. The other situation occurred for wear particles for fatigue, and adhesion, under loads of 30 and 50 N, and scuffing, where the levels of several further harmonics are distinctly higher. The spectra of adhesive wear particles, under a load of 50 N, and scuffing wear particles, under a load of 1000 N, differ from the remaining particles in higher levels of harmonics typical for more complex textures. For example, the twelfth component of wear particles, adhesion under load of 50 N and scuffing under load of 1000 N, is 100 and 118, and the remaining particles are in a range from 64 to 82.

The numbers in parentheses are the standard deviation values for five particles.

The majority of the analysed harmonic components are characterised by the high variability within each kind of particle. Generally, considering standard deviation values shown in the comparisons, one should regard them as large. It also shows the coefficient of variation values (relative deviation standard), which is from 14 to 93% for dominant harmonic components and from 22 to 78% for the remaining harmonics. On account of variety of features of the considered image and the possibility of the occurrence of deformation and noise, the methods of automatic classification of spectra can be use for further analysis of the variability of measurement data.

Table 3. Average values of harmonic components of wear particles amplitude spectra
 Tabela 3. Wartości średnie składowych harmonicznych widm amplitudowych badanych cząstek zużycia

No.	Wear particle type	Component number															
		1	2	3	4	5	6	7	8	9	10	11	12	13	14	15	16
1	Adhesive wear particles – load 10 N	0	158 (58)	214 (56)	178 (98)	79 (58)	80 (52)	90 (51)	51 (38)	55 (42)	63 (11)	36 (25)	38 (14)	23 (16)	24 (8)	22 (11)	14 (4)
2	Adhesive wear particles – load 30 N	0	215 (51)	183 (59)	138 (55)	166 (75)	131 (104)	109 (101)	76 (34)	100 (60)	45 (14)	84 (33)	82 (62)	57 (35)	76 (40)	57 (30)	64 (32)
3	Adhesive wear particles – load 50 N	0	186 (82)	222 (62)	120 (17)	112 (60)	146 (67)	110 (94)	123 (94)	142 (90)	84 (32)	83 (38)	100 (72)	83 (62)	63 (45)	54 (32)	47 (36)
4	Scuffing wear particles – load 500 N	0	159 (60)	174 (48)	211 (65)	137 (44)	116 (67)	83 (50)	75 (47)	92 (47)	69 (32)	79 (37)	66 (31)	31 (13)	36 (16)	27 (15)	26 (19)
5	Scuffing wear particles – load 1000 N	0	172 (70)	135 (84)	198 (64)	131 (21)	138 (73)	154 (57)	99 (49)	91 (45)	171 (61)	97 (68)	118 (47)	70 (30)	78 (32)	75 (23)	53 (34)
6	Abrasive wear particles	0	219 (49)	187 (86)	131 (71)	91 (47)	80 (26)	67 (21)	49 (35)	36 (9)	33 (9)	34 (19)	30 (8)	22 (11)	20 (12)	23 (12)	16 (11)
7	Fatigue wear particles – load 50 N	0	144 (89)	160 (100)	108 (88)	148 (66)	126 (76)	78 (35)	81 (26)	66 (34)	77 (39)	46 (10)	64 (33)	55 (23)	44 (23)	42 (18)	49 (13)
8	Fatigue wear particles – load 100 N	0	206 (67)	203 (75)	90 (57)	111 (71)	91 (34)	99 (50)	110 (63)	112 (45)	85 (35)	99 (64)	77 (52)	79 (51)	53 (18)	52 (30)	41 (32)

6. Fractal dimension

On Figures 5 and 6, the fractal analysis examples of wear particles contour by chord method were presented. In Table 3 and on Fig. 7, the average values of the fractal dimensions for the groups of particles obtained in different processes of wear are indicated. The number of the investigated particles in each group of particles was 10. The fractal analysis showed that there are differences in the degree of complexity of wear particle contour. As can be seen from Table 3 and Fig. 7, that a wear particle with fatigue under a load of 100 N and adhesion under a load of 30 and 50 N have a greater the fractal dimension (1.16, 1.14 and 1.14) in comparison with other wear particles with scuffing under a load of 500

N, adhesion under a load 10 N and abrasion (fractal dimension = 1.09, 1.10 and 1.10). The obtained values differ depending on the size of load in the given tribological test. The increase in load causes the rise of the particles' fractal dimension. The fractal dimension of scuffing wear particles under a load of 500 N is 1.09, and under load of 1000 N, it increases to 1.12. The greater value of the particles' fractal dimension means a greater degree of the complexity of their contour. Hence, the information concerning the wear mechanism and the intensity of friction couple elements can be obtained on the basis of the fractal dimension. It is possible to improve the efficiency of the described approach by taking into consideration fractal features of particles. However, this requires the use of better solutions in research methods, including equipment and software.

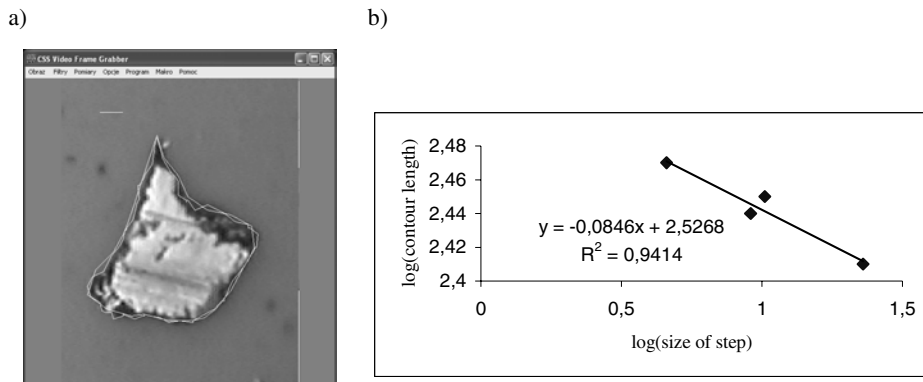


Fig. 5. The determination of the fractal dimension of the scuffing wear particles under a contact load of 500 N. The particle with marked break line (a) and regression line for relation $\log[L(x)]$ and $\log x$ (b)
Rys. 5. Wyznaczenie wymiaru fraktalnego cząstki zużycia scuffingowego przy obciążeniu 500 N. Cząstka z naniesioną linią łamaną (a) i linia regresji dla zależności $\log[L(x)]$ od $\log x$ (b)

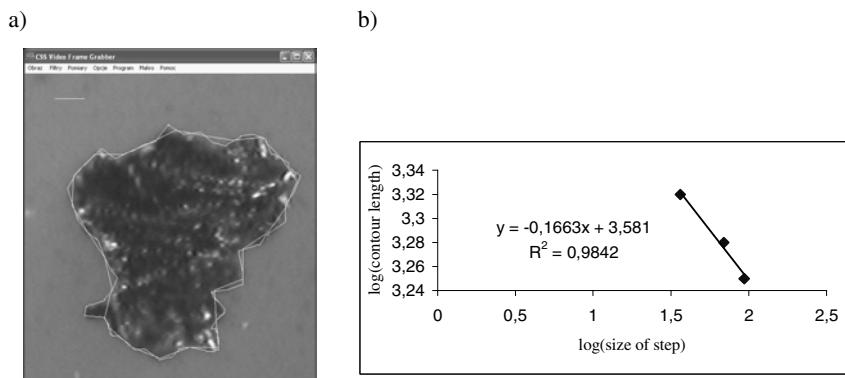


Fig. 6. The determination of the fractal dimension of the scuffing wear particles under a contact load of 1000 N. The particle with marked break line (a) and regression line for relation $\log[L(x)]$ and $\log x$ (b)
Rys. 6. Wyznaczenie wymiaru fraktalnego cząstki zużycia scuffingowego przy obciążeniu 1000 N. Cząstka z naniesioną linią łamaną (a) i linia regresji dla zależności $\log[L(x)]$ od $\log x$ (b)

Table 3. Average values of the fractal dimension for investigated types of particles
Tabela 3. Zestawienie wartości średnich wymiarów fraktalnych badanych rodzajów cząstek zużycia

No.	Wear particle type	Fractal dimension	Standard deviation
1	Adhesive wear particles – load 10 N	1.10	0.05
2	Adhesive wear particles – load 30 N	1.14	0.09
3	Adhesive wear particles – load 50 N	1.14	0.07
4	Scuffing wear particles – load 500 N	1.09	0.08
5	Scuffing wear particles – load 1000 N	1.12	0.05
6	Abrasive wear particles	1.10	0.07
7	Fatigue wear particles – load 50 N	1.13	0.07
8	Fatigue wear particles – load 100 N	1.16	0.06

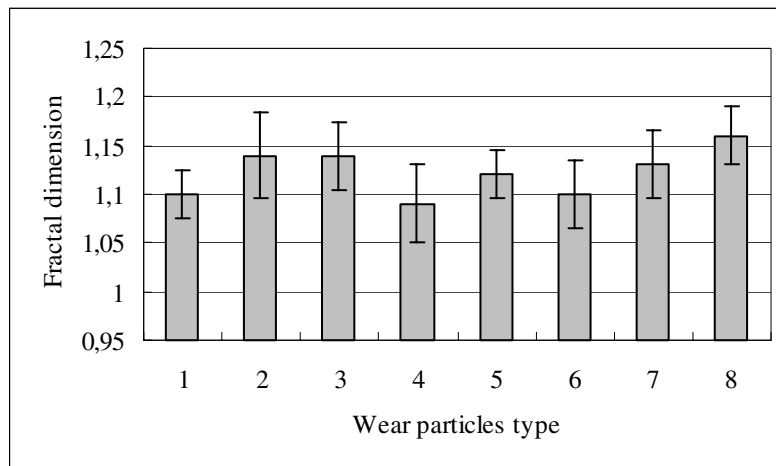


Fig. 7. The graph of the average values of the fractal dimension for the investigated types of the wear particles: adhesion under load of 10 N (1), 30 N (2), 50 N (3), scuffing under load of 500 N (4), 1000 N (5), abrasion (6) and fatigue under load of 50 N (7) and 100 N (8)

Rys. 7. Wykres wartości średnich wymiarów fraktalnych cząstek zużycia adhezyjnego przy obciążeniu styku 10 N (1), 30 N (2), 50 N (3), scuffingowego przy obciążeniu styku 500 N (4), 1000 N (5), ściernego (6) i zmęczeniowego przy obciążeniu styku 50 N (7) i 100 N (8)

7. Conclusions

The conducted research indicates that the application of the computer image analysis of wear particles in the exploitation diagnostics field of machines and technical devices enables the estimation of the current technical state of a tribological system and the prognosis of its further changes. Taking into account the development capabilities of the method, it was found that it can become an important tool for estimation of the state of friction couple in real conditions. The determination of morphological parameters opens the possibilities of the creation of databases and full documentation of the course of the wear process.

The significant practical significance of this research is connected with the application of the computer image analysis system equipped with a commonly available and applied optical microscope. The colour images of wear particles obtained with the microscope can be a carrier of information that is important from the point of view of technical diagnostics about investigated material associations. The information obtained in this way, in connection with the analysis of the construction of friction couple, and the conditions of its work, provide the possibility of the determination of the kind and state of the material of the particles and the place, reasons, and manner of their formation. By applying unified equipment and software, it will be possible to retain the comparability of research results obtained in different laboratories.

The further research for the purposes of the verification of the developed procedures, through research of wear processes running in real tribological systems, will allow the utilisation these procedures in developing a diagnosis system. In this operation, different artificial intelligence methods can be used enabling fast and unequivocal wear particle identification and the wear mechanism. The achievements in the field of electronics and informatics give the opportunity for more detailed particle research, exact analysing of the results and, on this basis of providing users information and recommendations connected with further exploitation, provide a manner for making repairs.

The results of the conducted research indicate the possibility of the application of the computer image analysis of wear particles at the stage of newly developed tribological systems as well as the time of their exploitation. It should be useful, especially in case of the large technical objects, being a single solution or by producing a short series where emergency states present a significant danger to safety and may bring serious economic losses.

References

- [1] Hunt T.M.: Handbook of wear debris analysis and particle detection in liquids, Elsevier Science Publishers LTD (1993).

- [2] Bovik A.: Handbook of image and video processing, Academic Press, San Diego (2000).
- [3] Hamblin M. G., Stachowiak G. W.: A multi – scale measure of particle abrasivity, *Wear* 185, 225–233 (1995).
- [4] Myshkin N.K., Kong H., Grigoriev A.Y. Yoon E.-S.: The use of color in wear debris analysis, *Wear* 251, 1218–1226 (2001).
- [5] Shirong G., Guoan Ch., Xiaoyun Z.: Fractal characterization of wear particle accumulation in the wear process, *Wear* 251, 1227–1233 (2001).
- [6] Stachowiak G.W., Kirk T.B., Stachowiak G.B.: Ferrography and fractal analysis of contamination particles in unused lubricating oils, *Tribology International* 24, 6, 329–334 (1991).
- [7] Stachowiak G.W., Podsiadło P.: Surface characterization of wear particles, *Wear* 225–229, 1171–1185 (1999).
- [8] Tadeusiewicz R., Korohoda P.: Computer image processing and analysis, FPT, Kraków (1997) (in Polish).
- [9] Wojnar L., Kurzydłowski K.J., Szala J.: Practice of image analysis, Polskie Towarzystwo Stereologiczne, Kraków (2002) (in Polish).
- [10] Wrona M.: Description of morphology features of wear particles with the use of a digital analysis image system, *Problemy Eksploatacji* 1, 135–145 (2004) (in Polish).
- [11] Wrona M.: Possibilities of using of the colour in wear particles analysis, *Tribologia* 3, 351–361 (2005) (in Polish).
- [12] Wrona M.: Quantitative analysis of wear particles texture using computer image analysis, *Tribologia* 4, 181–190 (2006) (in Polish).
- [13] Zieliński K.W., Strzelecki M.: Computer analysis of biomedical image. An introduction to morphometry and quantitative pathology, PWN, Warszawa (2001) (in Polish).
- [14] Szczerek M., Wiśniewski M. (red.): Tribology and tribotechnics, ITeE, Radom (2000) (in Polish).

Zastosowanie komputerowej analizy obrazu w badaniach cząstek zużycia

Streszczenie

W pracy zbadano możliwości zastosowania komputerowej analizy obrazu do charakteryzowania tekstury, barwy i konturu cząstek zużycia. Oceny tekstury i barwy i cząstek zużycia dokonano na podstawie analizy zmian jasności i poszczególnych składowych wybranych modeli barw: RGB, HSB i CIE $L^*a^*b^*$. W opisie statystycznym rozkładów zastosowano wiele parametrów, takich jak: wartość średnia, odchylenie standardowe, mediana, skośność, kurtoza. Przeprowadzono również ocenę tekstury powierzchni i konturu cząstek zużycia metodą analizy Fouriera i fraktalną. Za pomocą jednowymiarowej, szybkiej transformaty Fouriera (FFT) określono parametry liczbowe widma amplitudowego dla punktów wybranego odcinka naniesionego na obraz cząstki. W oparciu o odpowiednio przygotowane dane uzyskane z obrazów wyznaczono wymiar fraktalny konturu badanych cząstek z wykorzystaniem metody cięciw. Oceniono przydatność wyznaczonych parametrów przy ustalaniu przynależności cząstek zużycia do odpowiedniego typu. Na podstawie analizy uzyskanych wyników badań poszczególnych grup cząstek zużycia wyznaczono zależności pomiędzy cechami morfologicznymi cząstek zużycia a mechanizmami występującego zużycia węzłów tarcia.

HENRYK TOMASZEK ^{*}, SŁAWOMIR STĘPIEŃ ^{**}, MARIUSZ WAŻNY ^{**}

Aircraft flight safety with the risk of failure during performance of an aviation task

Key words

Reliability, safety, risk, failure, safety system, event, probability.

Słowa kluczowe

Niezawodność, bezpieczeństwo, ryzyko, awaria, układ zabezpieczający, zdarzenie, prawdopodobieństwo.

Summary

This article presents the outline of a method for the assessment of aircraft flight safety with the risk of failure. Despite efforts, appliance failures can occur. Appliance failures result in dangerous situations during flight. Cases of failures contribute to actions that have initiated the incorporation of backup systems into operations. These systems are aircraft units designed to

^{*} Air Force Institute of Technology, Księcia Bolesława Street 6, 01-494 Warsaw, Poland, phone: (22) 685-19-56.

^{**} Military University of Technology, Faculty of Mechatronics, gen. S. Kaliskiego Street 2, 00-908 Warsaw, Poland, phone (22) 683-77-89, (+22) 683-76-19.

prevent dangerous situations during flight. Moreover, they enable saving either an aircraft from damage or the crew in case of military aircraft. Backup systems include the following events:

- remaining in a state of operational readiness;
- taking over the function of a basic system after its damage;
- enabling landing of an aircraft or saving a pilot's life.

The article describes the above mentioned events and presents formulas for determining the probability of these events and formulas for the assessment of aircraft flight safety with the risk of aircraft failure.

1. Introduction

Flight safety is one of the most important undertakings in military and civil aviation. Despite efforts of technical services, appliance failures may occur. These failures cause dangerous situations during flight and force safety systems to take over some functions. These systems are integral units of aircraft. Safety systems are designed to prevent dangerous situations. They enable saving either an aircraft or the crew (a pilot) in case of military aircraft.

Safety systems require a special treatment during aircraft operation. This comes down to the following:

- maintaining them in a suitable operational readiness in case of basic unit failure, and
- taking over basic unit functions at the right time that guarantees aircraft efficiency.

The effectiveness of safety systems depends mainly on the following:

- 1) their technical state at the moment of the need to use them (i.e. operational readiness),
- 2) their operational reliability during their usage under conditions provided by a manufacturer, and
- 3) security of opportunity to save an aircraft, i.e. landing.

The performance of a task by a safety system (or safety systems) concerns the following events [3]:

- A* – An event that a safety system (or safety systems) is mounted on an aircraft, where there is no damage at the moment of the need to use it, i.e. it is in its operational readiness.
- B* – An event that a safety system will operate without damage during failure and it will take over basic system functions at the right time, i.e. there will be a reliable takeover of functions of a damaged basic system by a safety system.
- C* – An event that safety systems with aircraft systems in working order will, and this enable a safe landing, i.e. saving an aircraft from destruction.

Based on the above issues, it shall be stressed that safety systems with aircraft systems in working order will perform an aviation task if all the above mentioned events occur and an aircraft is saved.

A measure of a pilot's effective behaviour is the probability of a task performance after the occurrence of failure. This probability can be determined in the following way:

$$P_s(\tau) = P(A) \cdot P(B/A) \cdot P(C/A \cap B), \quad (1)$$

where:

$P_s(\tau)$ – the probability of a pilot's effective performance at a given time τ resulting from the scale of failure;

$P(A)$ – the probability of the occurrence of the event A – safety systems will be ready to take over operation in case of danger;

$P(B/A)$ – the conditional probability of the occurrence of the event B on the condition of the occurrence of the event A . The computational formula has the following form [1]:

$$P(B/A) = \frac{P(A \cap B)}{P(A)}, \quad (2)$$

$P(C/A \cap B)$ – the conditional probability of the occurrence of the event C (the landing of an aircraft) on the condition of the occurrence of the event A and B ; The computational formula has the following form [1]:

$$P(C/A \cap B) = \frac{P(A \cap B \cap C)}{P(A \cap B)}, \quad (3)$$

Substituting the formulas (2) and (3) into the formula (1), we obtain

$$P_s(\tau) = P(A) \cdot \frac{P(A \cap B)}{P(A)} \cdot \frac{P(A \cap B \cap C)}{P(A \cap B)} = P(A \cap B \cap C), \quad (4)$$

Aircraft safety depends on aircraft reliability until the occurrence of failure and the effectiveness of saving an aircraft after failure. The effectiveness of saving an aircraft is determined by the formula (4), and including aircraft reliability, it can be presented in the following way:

$$P_{BS} = R(t) + (1 - R(t))P_s(\tau), \quad (5)$$

where:

- P_{BS} – the probability of aircraft safety with failure;
 $R(t)$ – the reliability of an aircraft till the occurrence of failure
 (t means the time of aircraft flight);
 $(1 - R(t)) = Q(t)$ – the probability of the occurrence of failure till the time t , i.e. in the range of flight $(0, t)$;
 $P_s(\tau)$ – the probability of saving an aircraft after failure.

Based on the above data, the determination of aircraft safety comes down to the determination of the above mentioned probabilities. For the purpose of simplifying the notation, the term “a safety system” will mean both a safety system and safety systems in the further part of this article.

2. Determining the probability of the operational readiness of a safety system – $P(A)$

The operational readiness of a safety system is subject to a suitable control during aircraft operation via the use of appropriate diagnostic procedures. A safety system undergoes repair in case of deviation from requirements. Therefore, we can distinguish (a) the operational readiness of a safety system when all parameters do not diverge from requirements, and (b) the state of unreadiness when conditions are not met and the safety system is exposed to risk.

A diagram of the maintenance of the readiness state of a safety system is presented in Fig. 1.

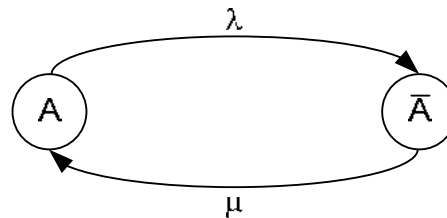


Fig. 1. Diagram of the maintenance of the readiness state of a safety system during aircraft operation: A – the readiness state of a safety system, \bar{A} – the unreadiness state of a safety system, λ – intensity of loss of the readiness state of a safety system, μ – intensity of the restoring of the readiness state

Rys. 1. Schemat utrzymania stanu gotowości układu zabezpieczającego w procesie eksploatacji statków: A – stan gotowości układu zabezpieczającego, \bar{A} – stan niegotowości układu zabezpieczającego, λ – intensywność utraty stanu gotowości układu zabezpieczającego, μ – intensywność przywracania stanu gotowości

Let $P(A, t)$ denote the probability of a safety system staying in the state “A,” and $P(\bar{A}, t) = 1 - P(A, t)$ the probability of a safety system staying in the state “ \bar{A} .” The time t is the time of a safety system staying in operation time. The probability $P(A, t)$ is the unknown quantity of the probability $P(A)$. The implemented notation aims at highlighting the variability of this probability in the function of time.

$$P(A, t) \equiv P(A).$$

The following equation of state is true [4]:

$$P(A, t + \Delta t) = [1 - \lambda \Delta t] P(A, t) + \mu \Delta t P(\bar{A}, t) + O(\Delta t), \quad (6)$$

where:

- $\lambda \Delta t \ll 1$ – the probability of the loss of the readiness state at the time interval Δt ;
- $[1 - \lambda \Delta t]$ – the probability of the lack of the loss of the readiness state of a safety system at the time interval Δt ;
- $\mu \Delta t$ – the probability of the restoring of the readiness state at the time interval Δt ;
- $O(\Delta t)$ – a small quantity of higher order.

After dividing both sides of the equation (6) by Δt and ordering the notion and after reaching the limit 0 by Δt , we obtain the following differential equation:

$$P'(A, t) = -\lambda P(A, t) + \mu P(\bar{A}, t). \quad (7)$$

Substituting in the equation (7) $P(\bar{A}, t) = 1 - P(A, t)$, we obtain the following equation:

$$P'(A, t) + (\lambda + \mu)P(A, t) = \mu. \quad (8)$$

The solution of the equation (8) is the probability of a safety system staying in the readiness state. It has the following form:

$$P(A, t) \equiv P(A) = \frac{\mu + \lambda e^{-(\lambda + \mu)t}}{\mu + \lambda}. \quad (9)$$

When $t \rightarrow \infty$, we obtain a stationary value of the probability of a safety system staying in the readiness state $P_{st}(A)$

$$P_{st}(A) = \frac{\mu}{\mu + \lambda} = K_g, \quad (10)$$

where: K_g - the readiness coefficient determined as the probability of a safety system staying in the readiness state.

It can be seen that the stationary value of the probability $P(A)$, i.e. $P_{st}(A)$, is the readiness coefficient K_g which is known from the theory of reliability.

3. Determining the probability of the event $P(B/A)$

For the purpose of determining the conditional probability $P(B/A)$, i.e. the occurrence of the event B under the condition of the occurrence of the event A , we will use deliberations from the Renewal Theory when renewal time is negligible. In our case, the probability $P(B/A)$ will be determined by the reliability of a device at a particular time interval (in this case, after the occurrence of failure).

This characteristic is significant for aeronautical devices that, in operational state, perform their functions only in a limited time (in this case, after the occurrence of failure).

Therefore, we will determine the probability of a failure-free operation of a safety system at a finite time interval $(t, t + \tau)$, where τ is the time of flight duration after failure. We will denote this probability by the following:

$$R_\tau(\tau) = P(B/A). \quad (11)$$

For the purpose of determining the searched probability, a set of independent events is implemented [5]:

$$\begin{aligned} A_0 &= \{t + \tau < T_1\}, \\ A_n &= \{t_n < t < t + \tau < t_n + T_{n+1}\} \quad n = 1, 2, \dots \end{aligned} \quad (12)$$

where:

- $n = 1, 2, \dots$ - subsequent damages during the time of use of a safety,
- T_i - random variables of duration of being in operational state (where $i=1, 2, \dots$),

t_n – moments of damages and at the same time repairs of a safety system ($n=1, 2, \dots$) determined on the axis of time.

The event A_0 means that there was no damage of a safety system until the moment t and at the time interval $(t, t+\tau)$.

The event A_n means that there were n damages until the moment t , and there were no damages at the time interval $(t, t+\tau)$.

The probability $R_t(\tau)$ is the probability of the occurrence of the event that is determined in the following way:

$$B = \bigcup_{n=0}^{\infty} A_n, \quad (13)$$

that is as follows:

$$R_t(\tau) = P(B) = \sum_{n=0}^{\infty} P(A_n). \quad (14)$$

In Paper [2], it was showed that we obtain the following integral equation from the relation (14)

$$R_t(\tau) = 1 - F(t+\tau) + \int_0^t [1 - F(t+\tau-x)]h(x)dx, \quad (15)$$

where:

$F(t)$ – the distribution function of the time of correct operation of a safety system,

$h(x)$ – the renewal density function.

The formula (15) is seldom used in practice, because we usually are interested in distant moments of time when the renewal process becomes stationary; thus, the probability $R_t(\tau)$ is no longer dependent on t . Therefore, in the equation (15), we use the transition to the limit $t \rightarrow \infty$.

In this situation, the component $1-F(t+\tau)$ of the formula (15) approaches 0 as t increases. For the purpose of finding the limit of the integral the following formula is used:

$$\lim_{t \rightarrow \infty} \int_0^t [1 - F(t+\tau-x)]h(x)dx. \quad (16)$$

We will use the renewal Theorem [2]. This theorem has the following content: if the time τ of the operation of an element has a continuous

distribution, and $Q(t)$ is a non-increasing monotone function and the integrable function is in the range $(0, \infty)$, then:

$$\lim_{t \rightarrow \infty} \int_0^t Q(t - \tau) dH(\tau) = \frac{1}{T_0} \int_0^t Q(x) dx, \quad (17)$$

where:

- T_0 – the expected value of the operation time of an “element,”
- $H(\tau)$ – the renewal function.

In our case, $Q(x)$ has the following form:

$$Q(x) = 1 - F(x + \tau). \quad (18)$$

Considering the above, from the formula (15), after transition $t \rightarrow \infty$, we obtain the following:

$$R(\tau) = \lim_{t \rightarrow \infty} R_t(\tau) = \frac{1}{\Theta} \int_0^\infty [1 - F(x + \tau)] dx. \quad (19)$$

Hence:

$$R(\tau) = \frac{1}{\Theta} \int_\tau^\infty [1 - F(t)] dt, \quad (20)$$

where: \bar{t} – the mean value of time till the damage of a safety system.

For constant intensity of damages of a safety system $\bar{\lambda}$, the relation (20) has the following form:

$$\begin{aligned} R(\tau) &= \frac{1}{\Theta} \int_\tau^\infty [1 - F(t)] dt = \frac{1}{\Theta} \int_\tau^\infty [1 - (1 - e^{-\bar{\lambda}t})] dt = \\ &= \frac{1}{\Theta} \int_\tau^\infty e^{-\bar{\lambda}t} dt = \frac{1}{\Theta} \left(-\frac{1}{\bar{\lambda}} e^{-\bar{\lambda}t} \right) \Big|_\tau^\infty = e^{-\bar{\lambda}\tau}. \end{aligned}$$

Therefore:

$$R(\tau) = e^{-\bar{\lambda}\tau}. \quad (21)$$

Using the relation (21) to assess the searched probability of the event B (i.e. that a safety system will perform a task), under the condition of the occurrence

of the event A (i.e. that a safety system was in working order at the moment when it was needed), the final formula has the following form:

$$P(B/A) = R(\tau) = e^{-\bar{\lambda}\tau}. \quad (22)$$

4. Determining the probability of the event C under the condition of the occurrence of the event A and B

If the event A and B occurred, then conditions for the event C are created, i.e. the landing of an aircraft.

The event C means that all systems and devices that guarantee the landing of an aircraft will operate without failures. For the purpose of determining this probability, we will use the intensity of damage [5]:

$$\chi(x) = \lim_{\Delta x \rightarrow 0} \frac{P(x < X \leq x + \Delta x / x < X)}{\Delta x}, \quad (23)$$

where:

- X – the random variable of time until the damage during landing (during the event C),
- x – the current value of the time of the course of landing,
- $P(x < X \leq x + \Delta x / x < X)$ – the conditional probability of the damage at the time interval $x < X \leq x + \Delta x$ under the condition that the random variable X is greater than x ,
- Δx – the increase of time during an aircraft landing.

The conditional probability can be presented in the following way:

$$P(x < X \leq x + \Delta x / X > x) = \frac{P(x < X \leq x + \Delta x)}{P(X > x)}. \quad (24)$$

Substituting (24) into (23), we obtain the following:

$$\chi(x) = \lim_{\Delta x \rightarrow 0} \frac{P(x < X \leq x + \Delta x)}{\Delta x P(X > x)}. \quad (25)$$

In the relation (25), after transition to the limit $\Delta x \rightarrow 0$, we obtain:

$$\chi(x) = \frac{f(x)}{R(x)} = \frac{-R'(x)}{R(x)}. \quad (26)$$

Hence, we obtain the following differential equation:

$$R'(x) + \chi(x)R(x) = 0, \quad (27)$$

where: $R(x)$ - the probability of the performance of the event C at the time interval $(0, x)$.

Assuming that the performance of the event C is $x = x_k$ and that the intensity of the damage during landing is the constant χ^* . Then

$$P(C/A \cap B) = R_{x_k} = e^{-\chi^* x_k}. \quad (28)$$

5. Final remarks

Using the obtained partial relations for the assumed events, we can provide combined relations for the safety of the flight of an aircraft with failure.

The effectiveness of saving an aircraft with a crew is determined with the formula (4). Hence, we obtain the following:

$$P_s(\tau) = \underbrace{K_g}_{P(A)} \cdot \underbrace{e^{-\lambda\tau}}_{P(B/A)} \cdot \underbrace{e^{-\chi^* x_k}}_{P(C/A \cap B)}. \quad (29)$$

We obtain the following relation for the safety of the flight of an aircraft with failure:

$$P_{BS} = \bar{R}(t + \tau) = R(t) + (1 - R(t))P_s(\tau), \quad (30)$$

where:

$P_s(\tau)$ - determined by the relation (29),

$R(t)$ - the reliability of the flight of an aircraft till the occurrence of failure.

The above-presented outline of the assessment of the safety of an aircraft with a crew requires further analysis aimed at the improvement of the obtained relations.

If an aircraft cannot be saved, it is possible to save a pilot's life with the use of a safety system in the form of an ejector seat. Similar logic patterns can be used to assess the chances of saving a pilot's life [3].

References

- [1] Abezgauz G.: Rachunek probabilistyczny. Poradnik. Wydawnictwo Ministra Obrony Narodowej, Warszawa 1973.
- [2] Gniedenko B.W., Bielajew J.K., Sołowiew A.D.: Metody matematyczne w teorii niezawodności. Wydawnictwo Naukowo-Techniczne, Warszawa 1968.
- [3] Szajnar S.: Wprowadzenie do oceny stanu gotowości do pracy i niezawodności użycia fotela katapultowego dla ratowania życia pilota. WAT Bulletin, Warszawa 2009 (article in press).
- [4] Tomaszek H., Żurek J., Stępień S.: Eksploatacja statku powietrznego z odnową i ryzykiem jego utraty. Zagadnienia Eksploatacji Maszyn, Book 4 (156), Radom 2008.
- [5] Tomaszek H., Wróblewski M.: Podstawy oceny efektywności eksploatacji systemów uzbrojenia lotniczego. Dom Wydawniczy Bellona, Warszawa 2001.

Manuscript received by Editorial Board, May 17th 2010

Bezpieczeństwo lotów statków powietrznych z ryzykiem awarii w czasie wykonywania zadania lotniczego

Streszczenie

W niniejszym artykule przedstawiono zarys metody oceny bezpieczeństwa lotu statku powietrznego z ryzykiem awarii. Pomimo starań zdarzają się awarie sprzętu, które są przyczyną niebezpiecznych sytuacji w locie. Przypadki awarii sprzętu przyczyniają się do podjęcia działań mających na celu włączenie do pracy układów pełniących rolę układów rezerwowych. Układy te są zespołami statku powietrznego przeznaczonymi do przeciwdziałania niebezpiecznym sytuacjom w locie. Ponadto umożliwiają one bądź to ratowanie statku powietrznego przed zniszczeniem, bądź tylko załogi w przypadku wojskowych statków powietrznych. Z układami zabezpieczającymi wiążą się następujące zdarzenia:

- pozostawanie w stanie gotowości do użycia;
- przejęcie funkcji układu podstawowego po jego uszkodzeniu;
- umożliwienie lądowania statku powietrznego lub tylko ratowanie życia pilota.

W artykule określono te zdarzenia i przedstawiono wzory do wyznaczenia ich prawdopodobieństw. Mając określone zależności na prawdopodobieństwo tych zdarzeń, podano wzory na szacowanie bezpieczeństwa lotu z ryzykiem awarii statku.

HENRYK TOMASZEK*, JÓZEF ŻUREK*, MARIUSZ WAŻNY**

Method of describing a catastrophic failure of an element of an aircraft

Key words

Crack initiation, fatigue, limit state, fatigue crack, reliability, catastrophic failure, risk.

Słowa kluczowe

Inicjacja pęknięcia, zmęczenie, stan graniczny, pęknięcie zmęczeniowe, niezawodność, uszkodzenie katastroficzne, ryzyko.

Summary

Failures resulting from fatigue processes are a dangerous type of aircraft damages.

This article presents an attempt to determine the probability of the occurrence of catastrophic failures of aircraft elements as a result of fatigue processes including basic stages, i.e. the crack initiation and the crack growth after the initiation in subcritical states.

The possibility to assess the probability of the occurrence of catastrophic failures in the function of the flying time is essential to develop control systems of a technical state of basic aircraft systems. In other words, it is essential for maintaining the required flight safety level. The probability of the catastrophic damage (failure) can be also considered as an element of the risk in the operation of aircraft.

* Air Force Institute of Technology, Księcia Bolesława Street 6, 01-494 Warsaw, Poland, phone (22) 685-19-56.

** Military University of Technology, Faculty of Mechatronics, gen. S. Kaliskiego Street 2, 00-908 Warsaw, Poland, phone: (22) 683-77-89, (22) 683-76-19.

1. Introduction

During the operation of aircraft, the construction undergoes a degradation process as a result of random load, which leads to failure. Fatigue of construction is the process of degradation. Catastrophic failures are caused by fatigue process [2, 3, 4]. Catastrophic failures are random events in the process of aircraft operation. They are rare but fraught with consequences.

It is assumed that the process of formation of catastrophic fatigue failures is characterised (in some cases) by certain stages. A simple course of fatigue process includes the following three basic stages:

- Crack initiation,
- Crack growth in subcritical state, and
- The destruction of the construction element after the exceeding of the critical crack length.

The formation process of the risk of catastrophic failure (in a particular case) begins with the crack initiation, which leads to the formation of a crack of a particular length. This crack relates to relations describing the crack growth, for example, the Paris formula.

The period in which the process of the crack initiation takes place is the stage that precedes the fundamental process of the crack growth until the critical value is reached. The critical value involves the destruction of the construction. Therefore, the stage of the crack initiation can be treated as the first stage of the destruction of the construction after which there is the second stage including the crack growth until the critical value is reached.

Therefore, it can be assumed that a parallel reliability structure of the destruction of the construction element is formed. The structure includes the crack initiation, then the subcritical crack growth, and the third stage, i.e. the catastrophic destruction of the construction.

2. Determining the probability of the crack initiation as a random process

We assume that the crack initiation in the element is caused by the accumulation of the degradation of an internal structure of the element as a result of the changing load. The changing load leads to accumulation of fatigue symptoms in different parts of the element, for example, various kinds of „obstacles”.

We assume that, among places where effects accumulate, there is one leading place in which the crack initiation occurs as a result of the accumulation of fatigue effects. As an example, near this selected “obstacle” dislocation, accumulation takes place.

Let Ψ be a parameter that is used to measure accumulated destructive symptoms of fatigue of the element structure surrounded by obstacles. Therefore, we can assume that a prognostic parameter for measuring the chance of the crack occurrence (its initiation) is the parameter Ψ . We digitise the prognostic parameter Ψ in the following way: $E_0, E_1, E_2, \dots, E_k, \dots$. We define these points as states of the process of the increase in fatigue effects before the crack initiation as a result of the action of load. Accumulated fatigue effects in the surrounding of the obstacle favour the crack initiation.

We assume that, in case of each state, there is a specific probability of the crack occurrence (the crack initiation). The probability of the crack initiation increases along with the increase in the state E_i ($i = 0, 1, 2, \dots$).

Figure 1 presents the increase in fatigue symptoms in the surrounding of the obstacle as a result of load, which connects with higher and higher state. A factor that forces the change of a state is the probability of the occurrence of the load cycle $\lambda\Delta t$, where λ is the intensity of the occurrence of the load cycle. In each state, there is probability of the crack initiation.

$$q_k(t) = (\mu_0 + k\mu)\Delta t \quad (1)$$

where: μ_0 – the intensity of the crack initiation at the initial moment,
 $k\mu$ – the intensity of the crack that depends on the state of accumulated fatigue effects.

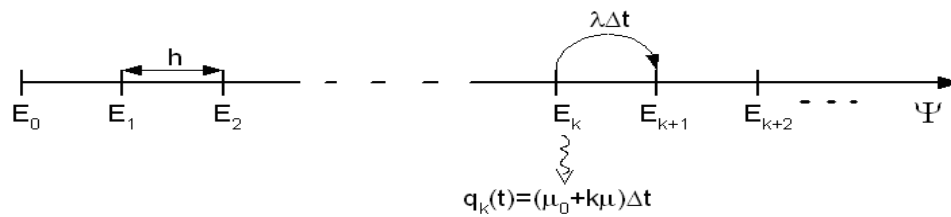


Fig. 1. Diagram of diagnostic parameter digitising: h – mean value of diagnostic parameter increase at the time Δt , $\lambda\Delta t$ – the probability of load cycle occurrence at the time Δt

Rys. 1. Schemat dyskretyzacji parametru diagnostycznego: h – średnia wartość przyrostu parametru diagnostycznego w czasie Δt , $\lambda\Delta t$ – prawdopodobieństwo pojawienia się cyklu obciążenia elementu w czasie Δt

Let $P_k(t)$ denote the probability that, at the moment t , the value of a diagnostic parameter reached the state E_k (where $k = 0, 1, 2, \dots$). Having the above assumptions, we can form the following set of equations (with infinite number of equations) [1, 5]:

$$\begin{aligned}
P_0(t + \Delta t) &= P_0(t)[1 - (\mu_0 + \lambda)\Delta t] + O(\Delta t), \\
&\vdots \qquad \text{for } k = 1, 2, \dots \quad (2) \\
P_k(t + \Delta t) &= P_k(t)[1 - (\mu_0 + k\mu + \lambda)\Delta t] + P_{k-1}(t)\lambda\Delta t + O(\Delta t)
\end{aligned}$$

After converting and dividing both sides of k – equation by Δt with the transition to the limit $\Delta t \rightarrow 0$, we obtain the following set of equations:

$$\begin{aligned}
P_0'(t) &= -(\mu_0 + \lambda)P_0(t), \\
&\vdots \qquad \text{for } k = 1, 2, \dots \quad (3) \\
P_k'(t) &= -(\mu_0 + \lambda + k\mu)P_k(t) + \lambda P_{k-1}(t)
\end{aligned}$$

Initial condition for each of these equations can be written in the following form:

$$P_i(0) = \begin{cases} 1 & \text{for } i = 0 \\ 0 & \text{for } i \neq 0 \end{cases} \quad (4)$$

Using a recursive method, we solve the set of equations (3).

Solution for $k = 0$

$$P_0'(t) = -(\mu_0 + \lambda)P_0(t),$$

$$\int_0^t \frac{P_0'(t)}{P_0(t)} dt = -\int_0^t (\mu_0 + \lambda) dt.$$

Hence,

$$P_0(t) = C_0 e^{-(\mu_0 + \lambda)t} \quad (5)$$

For $t = 0$, $P_0(0) = 1$ hence $C_0 = 1$.

Solution for any k

For any k , the differential equation has the following form:

$$P_k'(t) = -(\mu_0 + k\mu + \lambda)P_k(t) + \lambda P_{k-1}(t) \quad \text{for } k=1, 2, \dots \quad (6)$$

In this case, we provide the following solution:

$$P_k(t) = C_k(t) e^{-(\mu_0 + \lambda)t} \quad (7)$$

The derivative of the relation (7) has the following form:

$$P_k'(t) = C_k'(t) e^{-(\mu_0 + \lambda)t} + C_k(t) (-(\lambda + \mu_0)) e^{-(\mu_0 + \lambda)t} \quad (8)$$

Substituting the above equation into the relation (6), the following formula was obtained:

$$\begin{aligned} C_k'(t) e^{-(\mu_0 + \lambda)t} - (\lambda + \mu_0) C_k(t) e^{-(\mu_0 + \lambda)t} = \\ = -(\mu_0 + k\mu + \lambda) \frac{P_k(t)}{C_k(t) e^{-(\mu_0 + \lambda)t}} + \lambda \frac{P_{k-1}(t)}{C_{k-1}(t) e^{-(\mu_0 + \lambda)t}} \end{aligned}$$

Hence, we obtain the following equation:

$$C_k'(t) = -k\mu C_k(t) + \lambda C_{k-1}(t), \quad (9)$$

$$C_k'(t) + k\mu C_k(t) = \lambda C_{k-1}(t)$$

The equation (9) for $k=1$ will equal

$$C_1'(t) + \mu C_1(t) = \lambda \quad (10)$$

The general notation of the differential equation (10) has the following form:

$$y' + P(x)y = Q(x).$$

The solution of the relation is below:

$$y = e^{-\int_0^t P dx} \left(\int_0^t Q e^{\int_0^t P dx} dx \right) \quad (11)$$

Using Formula [11], we can write the solution of equation (10) in the following form:

$$\begin{aligned}
C_1(t) &= e^{-\int_0^t \mu dt} \left(\int_0^t \lambda e^{\int_0^t \mu dt} dt \right) = e^{-\mu t} \left(\int_0^t \lambda e^{\mu t} dt \right) = e^{-\mu t} \lambda \frac{1}{\mu} e^{\mu t} \Big|_0^t = \\
&= e^{-\mu t} \frac{\lambda}{\mu} (e^{\mu t} - 1) = \frac{\lambda}{\mu} - \frac{\lambda}{\mu} e^{-\mu t}
\end{aligned} \tag{11}$$

For $k = 2$, Equation [10] has the following form:

$$C_2'(t) = 2\mu C_2(t) = \lambda \left(\frac{\lambda}{\mu} - \frac{\lambda}{\mu} e^{-\mu t} \right) \tag{12}$$

The solution of the Equation [12]

$$\begin{aligned}
C_2(t) &= e^{-\int_0^t 2\mu dt} \int_0^t \lambda \left(\frac{\lambda^2}{\mu} - \frac{\lambda^2}{\mu} e^{-\mu t} \right) e^{\int_0^t 2\mu dt} dt = e^{-2\mu t} \left(\frac{\lambda^2}{\mu} \frac{1}{2\mu} e^{2\mu t} - \frac{\lambda^2}{\mu} \frac{1}{\mu} e^{2\mu t} \right) \Big|_0^t = \\
&= e^{-2\mu t} \left(\frac{\lambda^2}{2\mu^2} e^{2\mu t} - \frac{\lambda^2}{2\mu^2} - \frac{\lambda^2}{\mu^2} e^{\mu t} + \frac{\lambda^2}{\mu^2} \right) = e^{-2\mu t} \left(\frac{\lambda^2}{2\mu^2} e^{2\mu t} + \frac{2\lambda^2 - \lambda^2}{2\mu^2} - \frac{\lambda^2}{\mu^2} e^{\mu t} \right) = \\
&= \frac{\lambda^2}{2\mu^2} + \frac{\lambda^2}{2\mu^2} e^{-2\mu t} - \frac{\lambda^2}{\mu^2} e^{-\mu t} = \frac{\lambda^2}{2\mu^2} (1 + e^{-2\mu t}) - \frac{\lambda^2}{\mu^2} e^{-\mu t}
\end{aligned} \tag{13}$$

The equation describing the function was converted to the form that suggests the form of this function in a general case

$$C_2(t) = \frac{\lambda^2}{2\mu^2} + \frac{\lambda^2}{2\mu^2} e^{-2\mu t} - \frac{\lambda^2}{\mu^2} e^{-\mu t} \quad | \cdot 2,$$

$$2C_2(t) = \frac{\lambda^2}{\mu^2} - \frac{2\lambda^2}{\mu^2} e^{-\mu t} + \frac{\lambda^2}{\mu^2} e^{-2\mu t}.$$

Hence,

$$C_2(t) = \left(\frac{\lambda}{\mu} - \frac{\lambda}{\mu} e^{-\mu t} \right)^2 \frac{1}{2} \quad (14)$$

The form of the equation (14) enables us to provide the notion of the function in a general form. This relation has the following form:

$$C_k(t) = \frac{1}{k!} \left(\frac{\lambda}{\mu} - \frac{\lambda}{\mu} e^{-\mu t} \right)^k \quad (15)$$

Using (15), we can write the solution of the equation (6). These solutions have the following form:

$$P_k(t) = \frac{1}{k!} \left(\frac{\lambda}{\mu} - \frac{\lambda}{\mu} e^{-\mu t} \right)^k e^{-(\mu_0 + \lambda)t} \quad k = 1, 2, \dots \quad (16)$$

Using Relations (5) and (16), we can determine the reliability of the element (non-initiation of the crack). Hence:

$$R_1(t) = \sum_{k=0}^{\infty} P_k(t),$$

$$R_1(t) = \sum_{k=0}^{\infty} \frac{1}{k!} \left(\frac{\lambda}{\mu} - \frac{\lambda}{\mu} e^{-\mu t} \right)^k e^{-(\mu_0 + \lambda)t} \quad (17)$$

The following equality occurs:

$$\sum_{k=0}^{\infty} \frac{1}{k!} \left(\frac{\lambda}{\mu} - \frac{\lambda}{\mu} e^{-\mu t} \right)^k = e^{\frac{\lambda}{\mu} - \frac{\lambda}{\mu} e^{-\mu t}} \quad (18)$$

Using the relation (18), the formula for the reliability has the following form:

$$R_1(t) = e^{\frac{\lambda}{\mu} - \frac{\lambda}{\mu} e^{-\mu t}} e^{-(\mu_0 + \lambda)t}$$

Hence,

$$R_1(t) = e^{\frac{\lambda}{\mu}(1 - e^{-\mu t}) - (\mu_0 + \lambda)t} \quad (19)$$

Based on the above relation, the probability of the crack initiation for the flying time t will equal

$$Q_1(t) = 1 - e^{\frac{\lambda}{\mu}(1 - e^{-\mu t}) - (\mu_0 + \lambda)t} \quad (20)$$

3. Determining the relation for the crack growth after the occurrence of the crack initiation in the construction element

- 1) We assume the following [5, 6]:
 - After initiation, a small crack l_0 occurs in the construction element;
 - A technical state of the element is determined by one parameter in the form of the crack length. The current value of diagnostic parameter is marked with l ;
 - The change of the crack length can occur only during the operation of a device;
 - In the analysed case, the Paris formula has the following form:

$$\frac{dl}{dN_z} = CM_k^m (\sigma_{\max})^m \pi^{\frac{m}{2}} l^{\frac{m}{2}} \quad (21)$$

- where: c, m – material constants;
 N_z – the variable meaning the number of cycles in the assumed load spectrum;
 M_k – the coefficient of finiteness of dimensions of the element in the crack location;
 σ_{\max} – max. load that is determined by the relation (3).
- 2) It is assumed that a destructive factor is the load of the element in the form of the assumed load spectrum. We assume that this load spectrum enables determination of the following:
 - The total number of load cycles N_c during one flight (the standard cycle);
 - In the assumed spectrum, max. threshold loads are $\sigma_{\max}^1, \sigma_{\max}^2, \dots, \sigma_{\max}^L$ (we assume that there is L -thresholds in the load spectrum);

- The number of repetitions of determined load threshold values equals n_i , where

$$N_c = \sum_{l=1}^L n_l \quad (22)$$

- 3) Max. values of loads for the assumed thresholds are determined in the following way:

$$\sigma_{\max}^i = \bar{\sigma}_{sr}^i + \bar{\sigma}_a^i \quad (23)$$

where: σ_{\max}^i – max. value of load for i -threshold;
 $\bar{\sigma}_{sr}^i$ – mean value of load for i -threshold;

$$\bar{\sigma}_{sr}^i = \frac{\sigma_{\max}^i - \sigma_{\min}^i}{2}$$

$\bar{\sigma}_a^i$ – the amplitude of cyclic load for i -threshold.

- 4) Values of threshold load $\sigma_{\max}^1, \sigma_{\max}^2, \dots, \sigma_{\max}^L$ correspond to the following frequencies of their occurrence:

$$\frac{n_1}{N_c} = P_1; \quad \frac{n_2}{N_c} = P_2, \dots, \quad \frac{n_L}{N_c} = P_L,$$

where: $P_1 + P_2 + \dots + P_L = 1.$

Based on the above assumptions, we will attempt to determine the form of the density function of the crack length that depends on the time of the operation of an aircraft (flying time).

The relation (21) can be represented in the form of the function of the flying time of an aircraft. For this purpose, we assume the following:

$$N_z = \lambda t \quad (24)$$

where: λ – the intensity of the occurrence of load cycles in the assumed spectrum.
 t – the flying time of an aircraft.

In the assumed case

$$\lambda = \frac{1}{\Delta t}$$

where: Δt – mean time of fatigue cycle in the assumed spectrum.

We can assume a working formula for determining in the following form:

$$\Delta t = \frac{T}{N_c}$$

where: T – flight duration time of the standard cycle.

The relation (21) in the function of the flying time has the following form:

$$\frac{dl}{dt} = \lambda C M_k^m (\sigma_{\max})^m \pi^{\frac{m}{2}} l^{\frac{m}{2}} \quad (25)$$

The form of the solution of the equation (25) depends on the value of the index of the power m . In the considered case, we assume $m=2$. Hence, the equation (25) has the following form:

$$\frac{dl}{dt} = \lambda C M_k^2 (\sigma_{\max})^2 \pi l \quad (26)$$

The crack growth for the increase of the flying time Δt is:

$$\Delta l = \lambda C M_k^2 (\sigma_{\max})^2 \pi l \Delta t \quad (27)$$

Using the previous findings, we can determine the relation for the density function of the crack length in the function of the flying time of an aircraft. Let $U_{l,t}$ denote the probability that, at the moment t (for the flying time = t), the crack length will l . For the assumed notation, the dynamics of the crack length growth was described by the following differential equation:

$$U_{l,t+\Delta t} = \sum_{l=1}^L P_l U_{l-\Delta l}, t \quad (28)$$

$$\text{where: } \Delta l_1 = CM_k^2 (\sigma_{\max}^i)^2 \pi l \underbrace{\lambda \Delta t}_1; \quad i = 1, 2, \dots, L \quad (29)$$

P_i – the probability of the occurrence of, provided that $P_1 + P_2 + \dots + P_L = 1$.

The Equation (8) in the functional notation has the following form:

$$U(l, t + \Delta t) = \sum_{i=1}^L P_i U(l - \Delta l_i, t) \quad (30)$$

We convert the equation (10) to a partial differential equation. We assume the following approximations:

$$\begin{aligned} u(l, t + \Delta t) &\cong u(l, t) + \frac{\partial u(l, t)}{\partial t} \Delta t \\ u(l - \Delta l_i, t) &= u(l, t) - \frac{\partial u(l, t)}{\partial l} \Delta l_i + \frac{1}{2} \frac{\partial^2 u(l, t)}{\partial l^2} (\Delta l_i)^2 \end{aligned} \quad (31)$$

Substituting (31) into (30), we obtain the following:

$$\begin{aligned} u(l, t) + \frac{\partial u(l, t)}{\partial t} \Delta t &= \sum_{i=1}^L P_i \left\{ u(l, t) - \frac{\partial u(l, t)}{\partial l} \Delta l_i + \frac{1}{2} \frac{\partial^2 u(l, t)}{\partial l^2} (\Delta l_i)^2 \right\} \\ \frac{\partial u(l, t)}{\partial t} \Delta t &= - \frac{\partial u(l, t)}{\partial l} \sum_{i=1}^L P_i \Delta l_i + \frac{1}{2} \frac{\partial^2 u(l, t)}{\partial l^2} \sum_{i=1}^L (\Delta l_i)^2 P_i \end{aligned}$$

Hence

$$\frac{\partial u(l, t)}{\partial t} = - \underbrace{\frac{1}{\Delta t} \sum_{i=1}^L P_i \Delta l_i}_{\alpha(t)} \frac{\partial u(l, t)}{\partial l} + \frac{1}{2} \underbrace{\frac{1}{\Delta t} \sum_{i=1}^L P_i (\Delta l_i)^2}_{\beta(t)} \frac{\partial^2 u(l, t)}{\partial l^2} \quad (32)$$

where: $\alpha(t)$ – mean crack length growth per unit of time;

$\beta(t)$ – mean square of the crack length growth per unit of time.

The transformation of the coefficient $\alpha(t)$ of Equation (32):

$$\begin{aligned}\alpha(t) &= \frac{1}{\Delta t} \sum_{i=1}^L \Delta l_i = \frac{1}{\Delta t} \sum_{i=1}^L CM_k^2 P_i(\sigma_{\max}^i)^2 \pi l \lambda \Delta t = \\ &= \lambda CM_k^2 \pi l \underbrace{[P_1(\sigma_{\max}^1)^2 + P_2(\sigma_{\max}^2)^2 + \dots + P_L(\sigma_{\max}^L)^2]}_{E[\sigma_{\max}^2]} = \\ &= \lambda CM_k^2 \pi E[\sigma_{\max}^2] l\end{aligned}\quad (33)$$

where: $E[\sigma_{\max}^2]$ – the second moment of load of the construction element.

For the purpose of determining the relation for the crack length l from deterministic perspective, the following relation was used:

$$\frac{dl}{dt} = \lambda CM_k^2 \pi E[\sigma_{\max}^2] l.$$

Hence

$$\int_{l_0}^l \frac{dl}{l} = \int_0^t \lambda CM_k^2 \pi E[\sigma_{\max}^2] dt,$$

Therefore

$$l = l_0 e^{\lambda CM_k^2 E[\sigma_{\max}^2] \pi t},$$

We will denote

$$\begin{aligned}CM_k^2 \pi &= C_1 \\ C_1 E[\sigma_{\max}^2] &= \bar{C}_1\end{aligned}\quad (34)$$

The relation for the coefficient $\alpha(t)$ has the following form:

$$\alpha(t) = \lambda \bar{C}_1 l_0 e^{\lambda \bar{C}_1 t}\quad (35)$$

Acting in a similar way, we can determine the relation for the value of the coefficient $\beta(t)$. After transformations, the equation (32) has the following form:

$$\frac{\partial u(l,t)}{\partial t} = -\alpha(t) \frac{\partial u(l,t)}{\partial t} + \frac{1}{2} \beta(t) \frac{\partial^2 u(l,t)}{\partial l^2} \quad (36)$$

The special solution of the equation (36) is the density function of the crack length in the following form:

$$u(l,t) = \frac{1}{\sqrt{2\pi A(t)}} e^{-\frac{(l-B(t))^2}{2A(t)}} \quad (37)$$

where: $B(t)$ – mean value of the crack growth for the flying time t ;
 $A(t)$ – the variance of the crack length for the flying time t .

For the material constant $m=2$, coefficients $A(t)$ and $B(t)$ are the solution of integrals:

$$B(t) = \int_0^t \alpha(t) dt = l_0 (e^{\lambda \bar{C}_1 t} - 1) \quad (38)$$

$$A(t) = \int_0^t \beta(t) dt = \frac{1}{2} l_0^2 \bar{C}_1 \omega (e^{2\lambda \bar{C}_1 t} - 1) \quad (39)$$

where:

$$\omega = \frac{E[\sigma_{\max}^4]}{(E[\sigma_{\max}^2])^2}.$$

Using the previous findings, the reliability of the construction element is as follows:

$$R_2(t) \cong \int_{-\infty}^{l_{kr}} u(l,t) dl \quad (40)$$

where:

$$u(l,t) = \frac{1}{\sqrt{2\pi A(t)}} e^{-\frac{(l-B(t))^2}{2A(t)}}$$

Considering the Relations (38) and (39), we obtain the following form of the integrand in Relation (40):

$$u(l, t) = \frac{1}{\sqrt{2\pi \frac{1}{2} l_0^2 \bar{C}_1 \omega (e^{2\lambda \bar{C}_1 t} - 1)}} e^{-\frac{(l-l_0(e^{\lambda \bar{C}_1 t} - 1))^2}{l_0^2 \bar{C}_1 \omega (e^{2\lambda \bar{C}_1 t} - 1)}} \quad (41)$$

We standardise the random variable l . As a result of standardisation, we obtain the new random variable „ z ”. Its mean value equals 0 and its variance equals 1.

$$z = \frac{l - B(t)}{\sqrt{A(t)}}$$

After standardising the random variable, the Formula (23) has the following form:

$$R_2(t) \cong \int_{-\infty}^{\frac{l_{kr} - B(t)}{\sqrt{A(t)}}} \frac{1}{\sqrt{2\pi}} e^{-\frac{z^2}{2}} dz \quad (42)$$

4. Final relations for the assumed stages of the crack development

The reliability of the element including the stages of the crack development is as follows:

$$R(t) = R_1(t) + (1 - R_1(t))R_2(t) \quad (43)$$

The unreliability, i.e. a specific risk of catastrophic failure is as follows:

$$Q(t) = Q_1(t) \cdot Q_2(t) \quad (44)$$

The relations (43) and (44) can be written in the following form:

$$R(t) = R_1(t) - (1 - R_1(t)) \int_{-\infty}^{l_d < l_{kr}} u(l, t) da \quad (45)$$

$$Q(t) = (1 - R_1(t)) \int_{l_{kr}}^{\infty} u(l, t) da \quad (46)$$

It can be presented that the stages of the crack growth form a parallel reliability structure. Failure of a parallel structure occurs when its all elements are damaged. Hence, it can be written as follows:

$$Q(t) = (1 - R_1(t)) \int_{l_{kr}}^{\infty} u(l, t) da,$$

$$R(t) = 1 - (1 - R_1(t)) \int_{l_{kr}}^{\infty} u(l, t) da.$$

Hence, we obtain the following relation (43):

$$R(t) = R_1(t) + (1 - R_1(t)) \int_{-\infty}^{l_{kr}} u(l, t) da.$$

Considering only the probability, the risk of the catastrophic failure of the construction element, including the crack, will be determined by Relation (46).

The value of the possibility of failures of the construction can be used to develop a control system of a technical state of an aircraft in the function of the flying time.

References

- [1] Gerebach J.B., Kordoński Ch.B.: Modele niezawodnościowe obiektów technicznych. Wydawnictwo Naukowo-Techniczne, Warszawa 1968.
- [2] Kałmucki W.S.: Prognozowanie resursów detali maszyn i elementów konstrukcji. Kiszinier, 1989.
- [3] Smirnov N.N., Ickovicz A.A.: Obsluzivaniye i remont aviacionnej tehniki po sostojaniju. Transport 1980.
- [4] Tomaszek H., Wróblewski M.: Podstawy oceny efektywności eksploatacji systemów uzbrojenia lotniczego. Dom Wydawniczy – Bellona, Warszawa 2001.
- [5] Tomaszek H., Żurek J., Jaształ M.: Prognozowanie uszkodzeń zagrażających bezpieczeństwu lotów statków powietrznych. Warszawa 2008.
- [6] Tomaszek H., Klimaszewski S., Zieja M.: Zarys probabilistycznej metody wyznaczania trwałości zmęczeniowej elementów konstrukcji z wykorzystaniem wzoru Parisa i funkcji gęstości czasu przekroczenia stanu granicznego. 35th International Scientific Congress on Powertrian and Transport Means – European KONES 2009, Zakopane 2009.

Manuscript received by Editorial Board, May 17th 2010

Metoda opisu uszkodzenia katastroficznego elementu konstrukcji statku powietrznego

Streszczenie

Niebezpiecznym rodzajem uszkodzeń statków powietrznego są awarie konstrukcji na tle procesów zmęczeniowych.

W artykule podjęto próbę określenia prawdopodobieństwa powstawania uszkodzeń katastroficznego elementu konstrukcji w wyniku działania procesów zmęczeniowych, uwzględniając podstawowe etapy, tj. inicjacji pęknięcia elementu konstrukcji i rozwoju pęknięcia po inicjacji w stanach podkrytycznych.

Możliwość szacowania prawdopodobieństwa pojawiania się uszkodzeń katastroficznego w funkcji nalotu statku jest niezbędna dla opracowania systemów kontroli stanu technicznego podstawowych układów statku powietrznego dla zachowania wymaganego poziomu bezpieczeństwa lotów. Prawdopodobieństwo uszkodzenia katastroficznego (awarii) może być również przyjęte jako element składowy pojęcia ryzyka w eksploatacji statków powietrznych.